Model for Core Loss Prediction at High Frequency and High Flux Density

Jemimah C Akiror

A Thesis

in

The Department

of

Electrical and Computer Engineering

Presented in Partial Fulfillment of the Requirements

for the Degree of Master of Applied Science at

Concordia University

Montreal, Quebec, Canada

September 2012

CONCORDIA UNIVERSITY

SCHOOL OF GRADUATE STUDIES

This is to certify that the thesis prepared

By: Jemimah C Akiror

Entitled: Model for core loss prediction at high frequency and high flux density

and submitted in partial fulfillment of the requirements for the degree of

Master of Applied Science

complies with the regulations of the University and meets the accepted standards with respect to originality and quality.

Signed by the final Examining Committee:

_____ Chair
Dr. R. Raut

_____ Supervisor
Dr. P. Pillay

_____ Examiner
Dr. S. Willamson

_____ Examiner
Dr. S. Rakheja

Approved by _____
Dr. W. E. Lynch.
Chair Department of Electrical and Computer Engineering

September 2012

_____
Dr.Robin A.L . Drew
Dean, Faculty of Engineering and
Computer Science

Abstract

Model for Core Loss Prediction at High Frequency and High Flux Density

Jemimah Connie Akiror

Any reduction in the losses of a machine causes a very significant improvement in the overall machine efficiency especially in high rating machines. To reduce core losses in electrical machines, one needs to accurately quantify them and therefore select the appropriate material for a specific application. Although various models exist, the model to be implemented in machine design software is not only required to be accurate but also simple to implement and applicable over a wide range of frequency and flux density.

In this thesis, core loss best fit models are examined for accuracy in core loss prediction. An existing model is improved to better predict core losses over a wide range of both frequency and flux density while maintaining a somewhat simple algorithm. This model is also adapted for application in real machines that exhibit non sinusoidal flux density. Verification of the models is done on various materials by comparing the calculated loss to the measured loss. The overall performance of this model showed consistency with measured results. Predictions and results are presented.

The improved model is also used to calculate losses in a typical machine core using finite element analysis. Results showed that the losses obtained were consistent with Epstein measured results.

Also included in this thesis is the application of a new loss separation method on already existing core loss models to study the behavior of the core loss coefficients. The coefficients were found to vary with both frequency and flux density.

Acknowledgment

First of all the author would like to thank God for making this entire process possible. Appreciation also goes to her supervisor Dr.Pragasen Pillay for the opportunity to pursue this course of study, his patience, valuable guidance and financial support.

Thanks also go to the author's friends and colleagues for their help during this degree program.

The Author is indebted to her mother and entire family for their all-round support and encouragement.

Table of Contents

List of figures

List of Tables

Chapter 1

1.1 Introduction

Electrical machine efficiency has taken precedence in both machine design and operation. Various designs and methods of operation have been adopted in a bid to increase machine efficiency. The efficiency of electrical machines is generally defined as the ratio of the output power to the input power where the output power can be obtained by subtracting the effect of the losses on the input power. The efficiency of a standard motor is highly dependent on various factors like the machine design, age of the machine, loading and operating conditions among others. However the total losses in the machine can be attributed to copper losses, core losses, friction and windage losses and stray losses or hard to measure losses. In general some losses tend to vary with the load especially during operation and some losses remain fixed especially after design [1].

Core losses are simply defined as the losses in the form of heat and noise that occur in the core of a machine when it is exposed to an alternating magnetizing force. These losses are dependent on the frequency of operation and level of induction. They contribute about 15- 25% of the total losses in a motor [2] with purely sinusoidal excitation as shown in Fig 1.1. This percentage is even more for non-sinusoidal excitation. In general, core losses are reduced by:

- Using high permeability steel – this reduces on the coercivity and retentivity of the material therefore reducing the hysteresis loss.

- Using thinner steel laminations – this reduces on the eddy currents that flow in the core and hence the total losses
- Lengthening the core – this reduces the magnetic flux density in the material hence reduces the loss due to magnetic effects

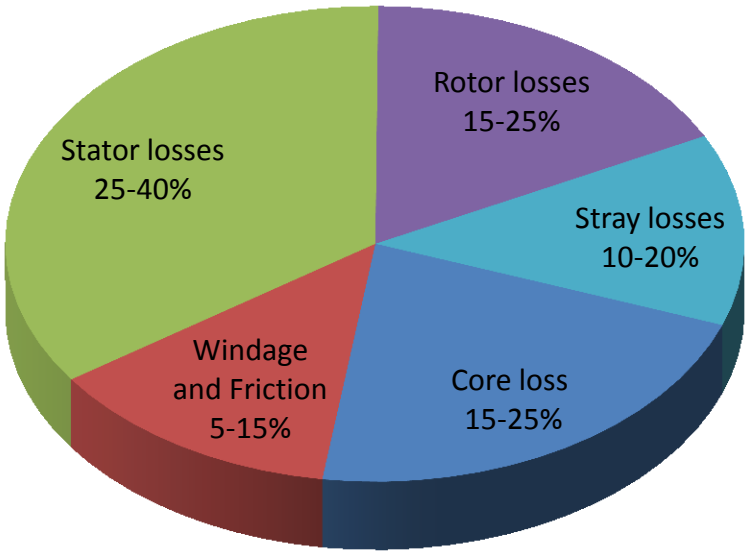

Fig 1.1 Typical loss percentages in an electrical machine.

As a step to further reduce these losses, one has to be able to effectively quantify them. This provides a basis for studying deferent technics that can be applied to reduce the losses for example annealing, using fully processed instead semi processed steel among others.

Quantifying core losses has therefore been a common point of interest for both engineers and physicists. Physicists have sought to understand the material's physical behavior under certain field excitation and mathematically model these phenomena to reproduce the hysteresis curve. Engineers on the other hand have sought easier approximations of this behavior for applications in machine design. This has led to the development of

various core loss models either based on physical characteristics occurring in the material or best fit models that sufficiently predict these losses.

With a core loss model that accurately predicts losses at different desired operating points and conditions, the machine designer is able to estimate the losses of the machine at the design stage therefore choosing a preferable material for the desired application.

1.2 Core loss prediction

Modeling of core losses has seen a resurgence of interest with continuous improvements in already existing models. The principal equation used to estimate core losses was first presented by Steinmetz [3] from which various models have been derived. The Steinmetz equation predicted core losses better for certain materials at different flux densities than others hence the need for model improvement. Modifications of the Steinmetz equation defined core loss as consisting of static hysteresis loss and dynamic eddy current loss. One of these modifications (1.1) allowed the calculation of the Steinmetz coefficient instead of having it as a universal constant n = 1.6 as in [3]. In this case the coefficient n was dependent on the values of flux density used to calculate it.

$$\begin{aligned} P_c &= P_h + P_e \\ &= K_h f B^n + K_e f^2 B^2 \end{aligned} \tag{1.1}$$

Where P_h and P_e are the hysteresis and eddy current losses respectively, f is the frequency and n is the Steinmetz coefficient, B is the flux density, K_h and K_e are the hysteresis and eddy current coefficients which depend on the lamination material, thickness, conductivity among other factors.

This model when used to predict core losses worked sufficiently well for some materials at flux densities less than 1T. At flux densities above 1T it gave a large variation between the measured and calculated loss. This model was inadequate for loss prediction in real machines because machines operate at higher flux densities. Also because many real machines operate at flux densities above 1T, this model was inadequate for loss prediction.

Another term called the excess loss in (1.2) was added to this formula to account for this difference between the measured and calculated core loss. Excess losses are explained as the 'losses due to the dynamic losses of the Weiss domains when a variable magnetic field is applied to the magnetic material' [4].

$$\begin{aligned} P_c &= P_h + P_e + P_a \\ &= K_h f B^n + K_e f^2 B^2 + K_a f^{1.5} B^{1.5} \end{aligned} \tag{1.2}$$

Where K_a is the excess loss coefficient dependent on the material thickness, cross sectional area, conductivity and a parameter which describes the material microstructure [5]. However since the eddy current losses cannot be separated from excess losses some authors argue that the core loss equation consists of only the hysteresis loss and eddy current loss components although the eddy current loss coefficient in this case also includes the excess loss coefficient. In [6] the authors instead of adding an excess loss term used a correction factor for the excess loss greater than 1 on the eddy current loss term. The eddy current, hysteresis and excess loss coefficients in various models were considered to vary with both frequency and flux density while other models considered them constant calculated from material properties. Core losses can also be obtained by using physics based models like the energetic Hysteresis model [7] and the Jiles Atherton

model [8] which model the hysteretic behavior (hysteresis loop) of a material from which the hysteresis loss can be obtained. Since this thesis emphasizes best fit models that make use of simple curve fitting techniques and experimental data, models [7] [8] [9] are beyond the scope of this thesis.

From (1.1) and (1.2) various models have been developed with different algorithms, limitations in the frequency and flux density ranges and different levels of accuracy. Since these models have to be implemented in machine design software, a more accurate and less complex algorithm model is indispensable.

The choice of stator and rotor material used in an electrical machine is just as important as the accuracy of the core loss model because it can directly be linked to the initial cost of the machine, its performance and quality. Magnetic steel cores are generally graded by their permissible losses and further classified into non-oriented steel, oriented steel, fully processed and semi processed steel [10]. These materials are produced to meet magnetic specifications dependent on their chemical composition. Steel cores usually contain alloys which increase the volume resistivity, affect the grain structure and have metallurgical effects that reduce the eddy current and hysteresis loss components. The alloys include silicon, aluminum, manganese while carbon, sulfur, nitrogen and phosphorous exist as impurities that can be reduced or eliminated by annealing semi processed steel. However of all the alloys, the amount of silicon greatly affects the total core loss of the material. Increasing silicon reduces the total core loss but also lowers the high induction permeability. Results have shown that even for the same material grade, core loss and maximum permeability also varies with the material thickness (gage). The materials with a thinner gage exhibit lower core loss and higher permeability.

1.3 Objective

The main objective of this thesis is to improve on a previous formulation of core loss prediction for use over a wide frequency and flux density range. This model should also be extended to non-sinusoidal field excitation given that at different points in real machines the pulsating flux is non-sinusoidal. The behavior of the core loss coefficients and their dependency on frequency and flux density will also be studied.

1.4 Summary

Since the accuracy of a model is determined by comparing its calculated loss to the measured loss, the method used to measure core loss is described in chapter 2. A review of some of the core loss formulas is done in chapter 3. Chapter 4 describes the calculation of the Steinmetz coefficients using a better method of loss separation. For extension of this model to non-sinusoidal flux density waveforms, it is converted into the time domain and used to calculate losses in Chapter 5. Chapter 6 concludes the thesis.

Chapter 2 Measurement of core losses

Core loss measurements have often been done by steel manufacturers to enable them classify their steel materials based on the properties obtained from the measurements. Usually this core loss data is provided at a few operating points for example at frequencies of 50Hz and 60Hz at 1T or 1.5T flux density. With this data, machine design software uses a model to predict the losses of a machine operating at user specified operating conditions. This core loss data is specific to the material, flux density and frequency.

2.1 Materials

Core loss measurements are made according to various acceptable standards [11] [12] [13] so that the materials irrespective of their manufacturer are standardized. Different steel manufacturers follow different standards and different nomenclature for their steel. However the material is considered the same provided properties like the core loss, permeability, resistivity and thickness are the same. Increasing the electrical resistance of the steel by alloying it with silicon and aluminum reduces the losses of the material while increasing its permeability. Non-oriented steel contains 0.5-3.25% Silicon and up to 0.5% Aluminum and 0.005% Carbon. High silicon percentages lower magnetostriction and together with other alloys decrease the curie temperature of the material. All these properties come together to define a specific material grade.

In this thesis AK(steel company) non oriented fully processed (FP) steel data was used for materials M15G29, M19G24, M19G29, M36G24 and M45G26. Table 2-1 shows

some of their electrical and physical properties [14]. The choice of these materials was based on the availability in the lab and also their applications.

Table 2-1 Material properties

Material(FP) Grades	Gage number	Thickness (mm)	Density (g/cc)	Core loss at 1.5T 60Hz	Resistivity (μΩ.cm)	Applications
M15	29	0.3556	7.65	1.45	50	LM,LG,LT
M19	29	0.3556	7.65	1.55	50	LM,LG,LT
M19	24	0.635	7.65	2	50	LM,LG,LT
M36	24	0.635	7.7	2.35	43	SM,SG,ST,LT,BI
M45	26	0.4699	7.75	2.4	37	SM,SG,ST,BI

SM, SG	Small Motor and Generators respectively (<100HP)
LM,LG	Large Motor and Generators respectively (>100HP)
ST	Small Transformers (<10KVA)
LT	Large transformers (>10KVA)
BI	Ballasts and ignition Coils

The material grade is the number that appears right after the letter M in the AISI nomenclature system. Low grade materials are always the desired materials because they have the highest resistivity and more silicon percentage hence the least core losses. For the same material it should also be noted that using a thinner lamination also reduces the losses as shown in the above by M19G24 and M19G29. Because of their properties, low grade materials are more expensive but very suitable for large machines applications. In large machines a small loss percentage saving is very significant.

2.2 Test Bench

The general setup for core loss measurements as shown in involves the exciting of a primary coil wrapped around a secondary coil directly on the lamination. Multiplying the input current in the primary coil and the output voltage from the secondary coil gives the total core loss of the lamination. The input current is responsible for the magnetic field strength (H) used to magnetize the sample and the measured output voltage indicates the level of magnetization flux density (B). From these two quantities the B-H curve of a material can be obtained and other properties like permeability calculated.

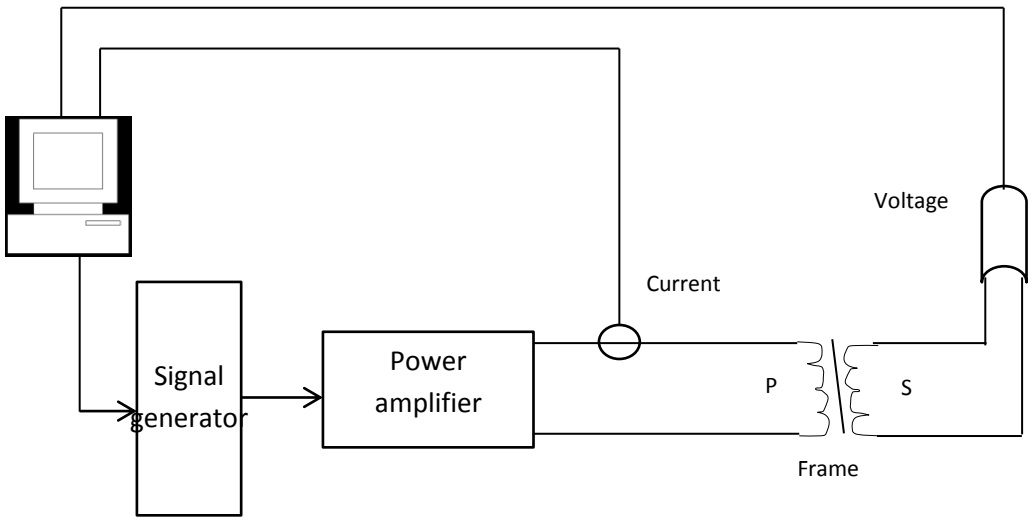

Fig 2.1 Core loss test bench

A commercial test system [15] was used to make the core loss measurements for the materials used in this thesis. The Donart system in Fig 2.2 comes with three types of testers, the Epstein tester, single sheet tester and the toroid tester. It consists of a computer, core loss testers, an amplifier, a signal generator and a power supply. Being a computer controlled set up, the signal commands are set by the user during the initialization of the test specifying levels of induction to be tested, the test frequency, the

effective magnetic path, density and width of the material, number and weight of the laminations used.

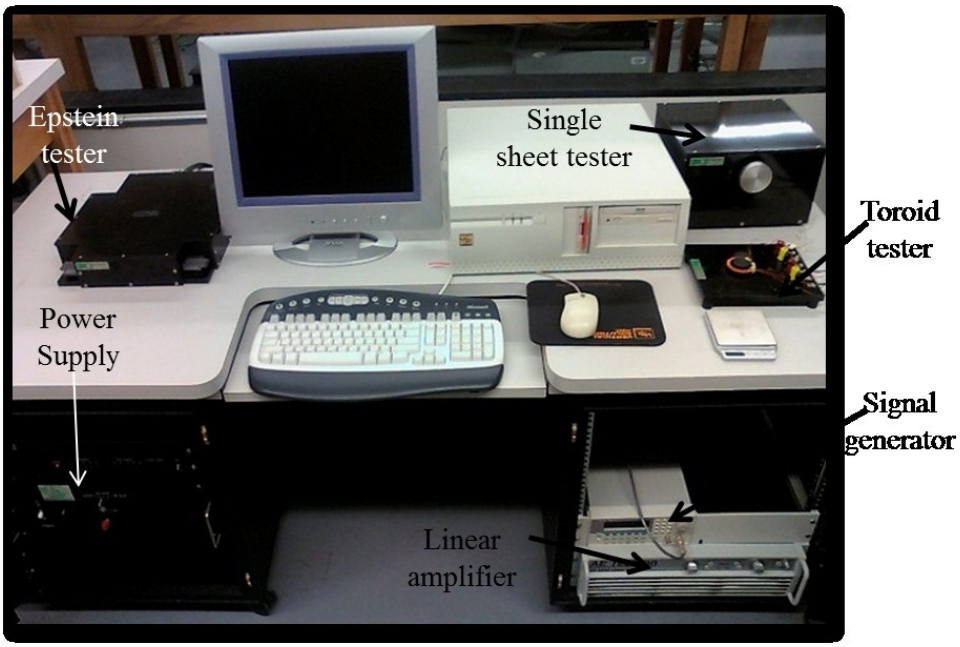

Fig 2.2 Donart Computer controlled test system

The signal is then sent to the signal generator that generates the required frequency of the signal and sends it to the amplifier for amplification thereafter used to excite the sample. There is a feedback signal that is used to ensure the waveform remains sinusoidal. Measurements of the input current and output voltage are then made from which the core loss can be derived. The tester is interfaced with the system and specifications of the type of test to be done are set. To start the test, the system first demagnetizes the sample to remove all residual flux in the sample and then starts magnetizing it to the specified induction levels while taking the core loss measurements and calculating permeability at each point until the material is saturated. The frequency range of this system is up to 4 kHz and flux density range is up to 2T, depending on the tester being used, the saturation

and temperature of the test material. These testers individually provide core loss data at different test frequencies, permeability and B-H loops which should ideally give the same core loss data for the same material.

In [16] [17] [18] the ASTM standard specifications for the material preparation, experimental setup and test methods for the toroid tester, single sheet tester (SST) and Epstein tester respectively are given. [19] and [20] give a summary of each of the testers including their advantages and disadvantages over each other.

2.3 Core loss Testers

2.3.1 Toroid tester

Laminations are cut into a ring shape according to ASTM standards and stacked together. Secondary windings are wound on the toroid followed by primary windings. The number of laminations stacked together and the test frequencies determine the number of turns required depending on the specifications of the amplifier. To increase the frequency measurement capability of the sample, the primary and secondary winding are made in pairs and connected in series to increase the number of turns for low frequency measurements. Fig 2.3 shows the toroid tester with the test sample ready for measurement.

This tester has a geometric similarity to a real motor or generator core and it forms a closed magnetic loop hence reduces the reluctance in the circuit due to the lack of an air gap however preparation of the sample is time consuming therefore is a less preferred method of core loss measurement.

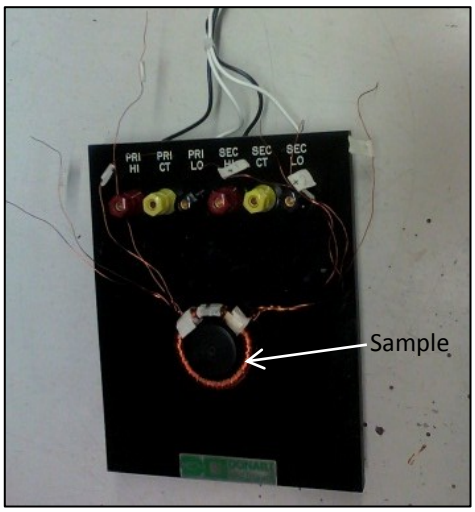

Fig 2.3 Toroid tester.

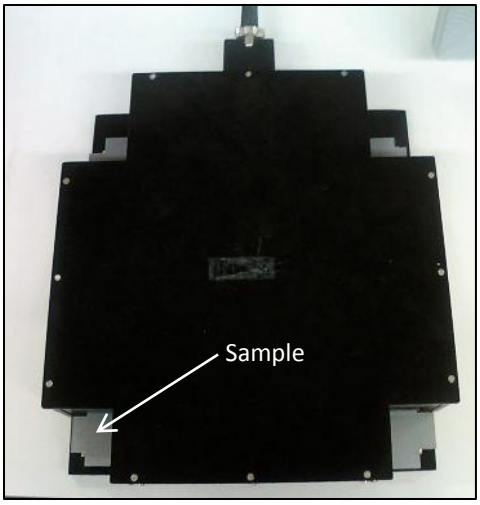

Fig 2.4 Epstein tester.

2.3.2 Epstein tester

Strips are cut according to the ASTM standard, the secondary and the primary windings are wound on the frame and the laminations placed inside the frame as shown in Fig 2.4. Laminations cut along the rolling direction should be placed opposite each other and those cut perpendicular to the rolling direction should be placed across from each other as well. The number of laminations should be a multiple of 4 such that each arm of the frame has the same number of laminations. Putting a large number of laminations especially for low frequency testing helps to reduce the magnetic reluctance and therefore give more accurate results. This is the most commonly used tester although it has its own drawbacks: it takes time to arrange the samples in the frame and magnetic reluctance exists due to the air gap between the laminations.

2.3.3 Single sheet tester

This method is commonly used by manufacturers for quality control especially since it uses one sample and therefore easy to assemble. However this tester requires calibration by using either the Epstein or toroid tester therefore exhibiting a dependence on other testers. Also because flux is only measured at the center of the strip this tester does not represent the material fully since only one strip is used. Fig 2.5 shows the single sheet tester (SST) with the test strip inserted in the frame. In comparison with the Epstein tester and toroid it is easier to set up and as with the toroid the air gap is reduced.

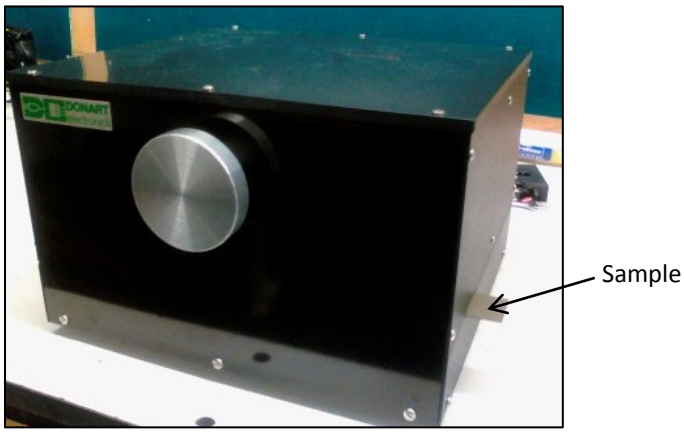

Fig 2.5 Single sheet tester.

2.4 Comparison of the testers

Core loss measurements taken from the different testers are ideally supposed to be the same for the same material. However this is not true hence the need to compare the results obtained from each of the testers. [19] and [14] show a comparison of the single sheet tester and the Epstein tester using different international standards, the technical aspects involved in each method and the poor correlation between their sample or

measurement parameters like the flux density, permeability, sample thickness and material grade.

[19] and [20] show a comparison of the Epstein tester and the toroid tester showing that the toroid tester generally gave a higher loss value than the Epstein tester at all the test frequencies used. This was explained by the toroid having higher hysteresis loss at lower frequencies due to reduced permeability from shearing stress and high eddy current losses at high frequencies.

In Fig 2.6 a comparison of the SST, toroid and Epstein testers is done using the total core loss measurements and permeability for M19G24.It was observed that the results for each of the testers were different although the SST and the Epstein testers were close while the toroid tester losses were a lot higher. The low permeability results of the toroid tester give evidence of the effects of stress on the toroid specimen.

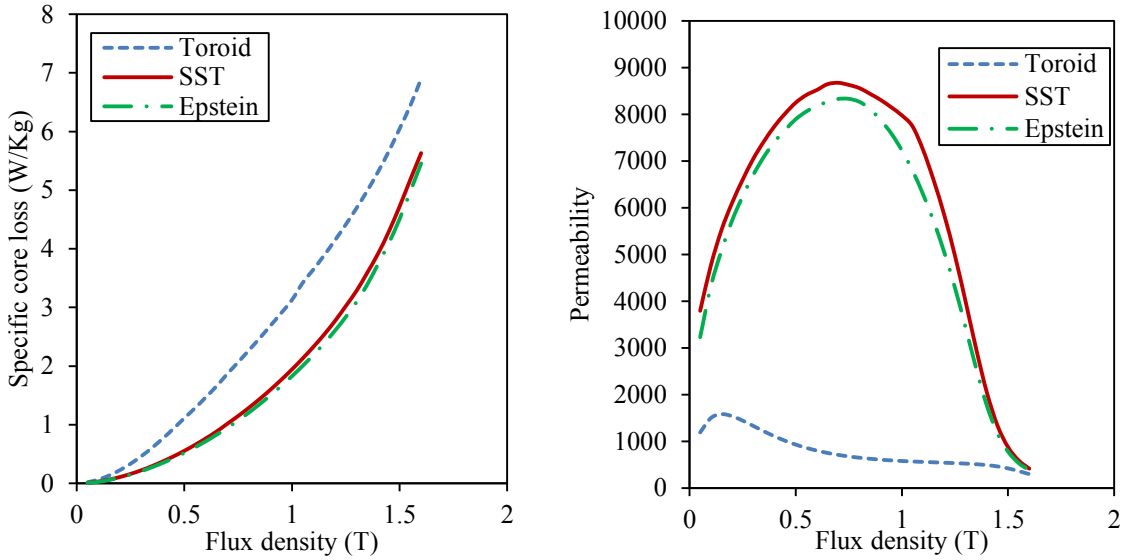

Fig 2.6 Comparison of the testers at 60Hz using M19G24.

Comparing these testers shows that whatever analysis is done using core loss data, stating the type of tester used is important especially for repeatability. In this thesis unless specified, all the analysis was done using the Epstein tester core loss data.

2.5 Summary

In this chapter, the test bench including the types of testers used to obtain core loss data has been presented. The materials whose data is used for analysis have been characterized and a comparison of the testers made.

Chapter 3 Core loss formulations

3.1 Review of core loss formulas.

Reviewing already existing formulas for core loss calculation is a good starting point before proposing a model since it allows one to know the trend in the modification of the models and provides a benchmark for whatever improvements are made. Starting from the Steinmetz equation (1.1) used to predict core loss up to 1T and at low frequencies, various modifications and improvements of the models have been made. To improve on the results obtained using (1.1), the Steinmetz coefficient was modified in [21] to a linear function of flux density $n = (a + bB)$ as in (3.1).

$$P_c = P_h + P_e \quad = K_h f B^{(a+bB)} + K_e f^2 B^2 \tag{3.1}$$

a and b are constants and material dependent.

To calculate core losses using (1.1) and (3.1) from the measured data, the specific core loss is divided by frequency to obtain specific core loss per cycle (3.2).

$$\frac{P_c}{f} \quad = \quad K_h B^n + K_e f B^2 \quad = D + Ef \tag{3.2}$$

Where $D = K_h B^n$ and $E = K_e B^2$. A plot of P_c/f vs f for different values of flux density and a linear curve fit is then made. K_e and K_h can then be calculated from D and E respectively with any two flux density values (3.3).

$$K_e = {}^{E}/_{B^2} \; ; \; \log D \; = \; \log K_h + n \, logB \tag{3.3}$$

For (3.1) three values of flux density are used instead of two as in the previous case. The predicted core loss can then be calculated when the hysteresis and eddy current coefficients are known.

For the two variations of core loss formulas above, the one with $n = (a + bB)$ numerically should give better results because it uses more data points. However since (1.1) and (3.1) were not suitable for calculation of core losses for flux densities greater than 1.0T and high frequencies because of the large variation between the calculated and measured loss. The excess loss component was added to the calculation (1.2), this involved making a quadratic fit of the specific core loss per cycle (3.4) verses square root of frequency.

$$\begin{aligned} \frac{P_c}{f} &= K_h B^n + K_e f B^2 + K_a f^{0.5} B^{1.5} \\ &= D + E (f^{0.5})^2 + G f^{0.5} \end{aligned} \tag{3.4}$$

Where $D = K_h B^n$, $E = K_e B^2$ and $G = K_a B^{1.5}$ and for given values of flux density coefficients K_h, K_e, K_a and n can be calculated using two data points.

In [22] the authors proposed a model for core loss prediction as a modification of (1.2) to better predict the losses hence (3.5).

$$\begin{aligned} P_c &= P_h + P_e + P_a \\ &= K_h f B^{(a+bB+cB^2)} + K_e f^2 B^2 + K_a f^{1.5} B^{1.5} \end{aligned} \tag{3.5}$$

$(a + bB + cB^2)$ represents the difference between the static hysteresis loop and the dynamic hysteresis loop mainly because the Steinmetz coefficient varies with flux density. The coefficients K_a and K_e were considered constant at all induction levels and K_h, a, b and c varied with frequency. After a quadratic fit (3.6) of the specific core loss per cycle verses the square root of frequency is made, the eddy current and hysteresis coefficients can be calculated from G and E.

$$\frac{P_c}{f} = K_h B^{(a+bB+cB^2)} + K_e f B^2 + K_a f^{0.5} B^{1.5}$$
$$= D + E(f^{0.5})^2 + G f^{0.5} \quad (3.6)$$

where $D = K_h B^{(a+bB+cB^2)}$, $E = K_e B^2$ and $G = K_a B^{1.5}$.With K_e and K_a known the eddy current loss and the excess loss can then be calculated and the hysteresis loss obtained by subtracting these losses from the total core loss. From (3.7) the hysteresis coefficients K_h and the Steinmetz coefficients a, b and c can then be calculated given four values of flux density.

$$logP_h = \log f + log\, K_h + (a + bB + cB^2) logB \quad (3.7)$$

All the models discussed above were reproduced to calculate core losses over a range of materials and their results compared to the measured losses obtained from experimental measurements.

Fig 3.1 - Fig 3.6 showed that (3.1) and (1.1) were not very different although numerically (3.1) using more data points should give more accurate results. (1.2) and (3.5) predicted the losses better than (1.1) and (3.1) with (3.5) indicating a better correlation between the measured and calculated loss using both low and high frequencies. These models where done on different types of materials to ensure repeatability and to confirm their individual trend of behavior.

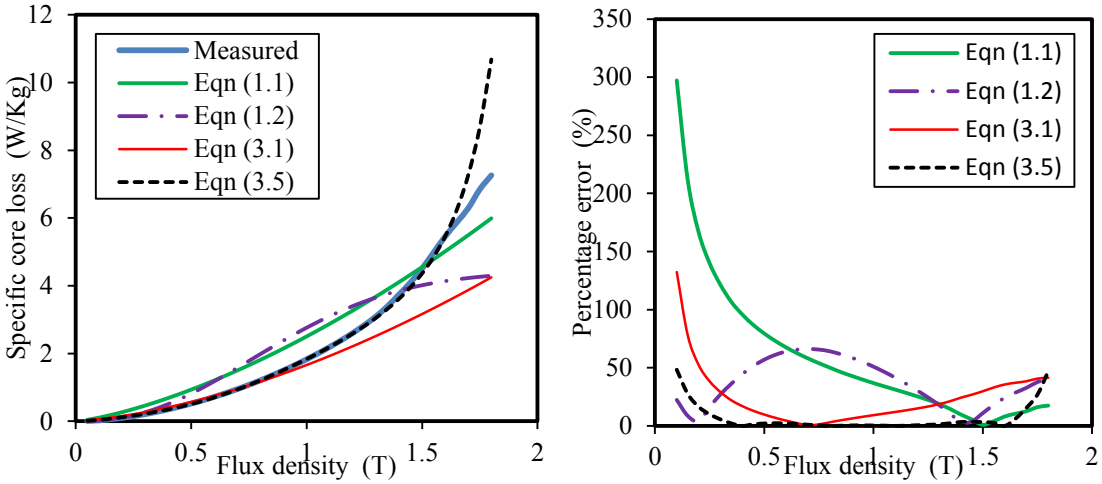

Fig 3.1 Specific core loss and percentage error vs flux density for M19G24 at 60Hz.

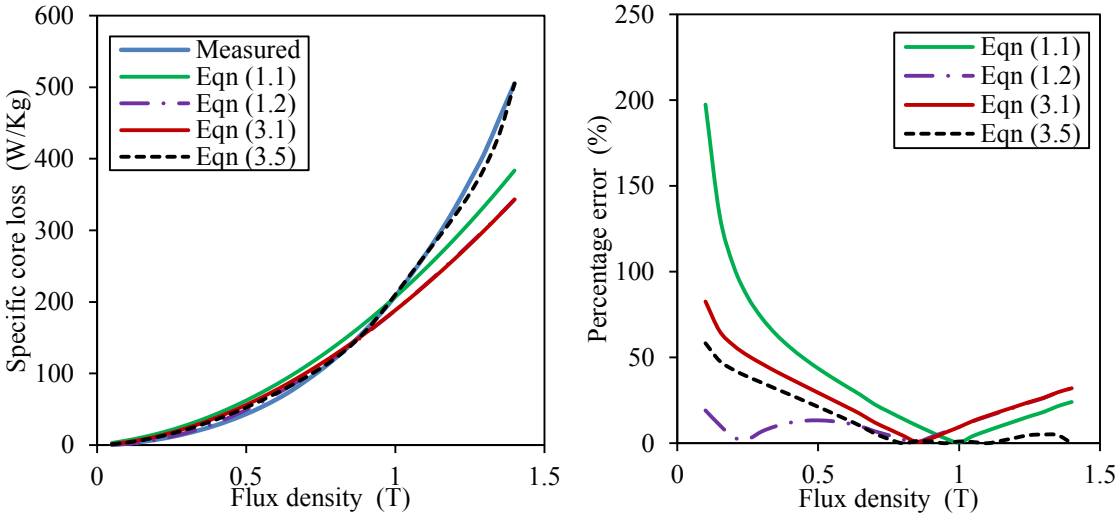

Fig 3.2 Specific core loss and percentage error vs flux density for M19G24 at 1kHz.

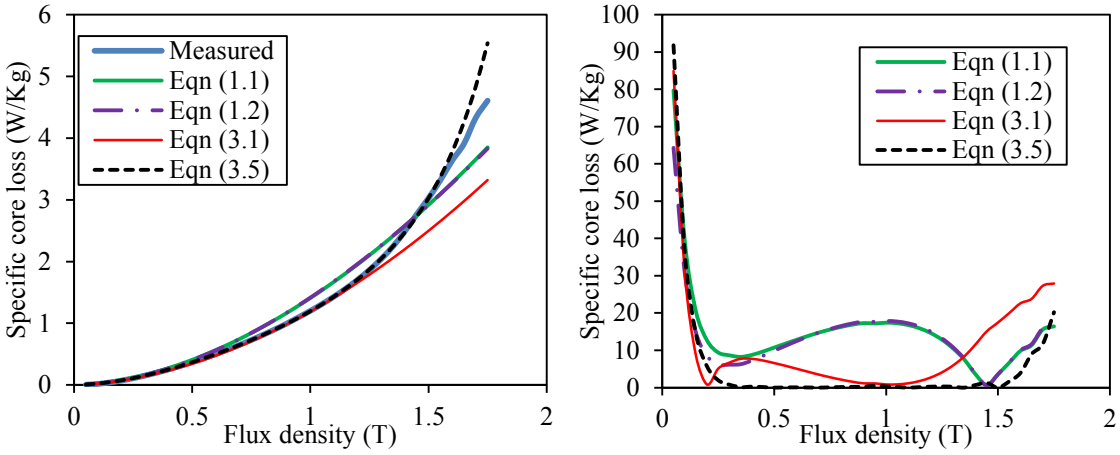

Fig 3.3 Specific core loss and percentage error vs flux density for M19G29 at 60Hz.

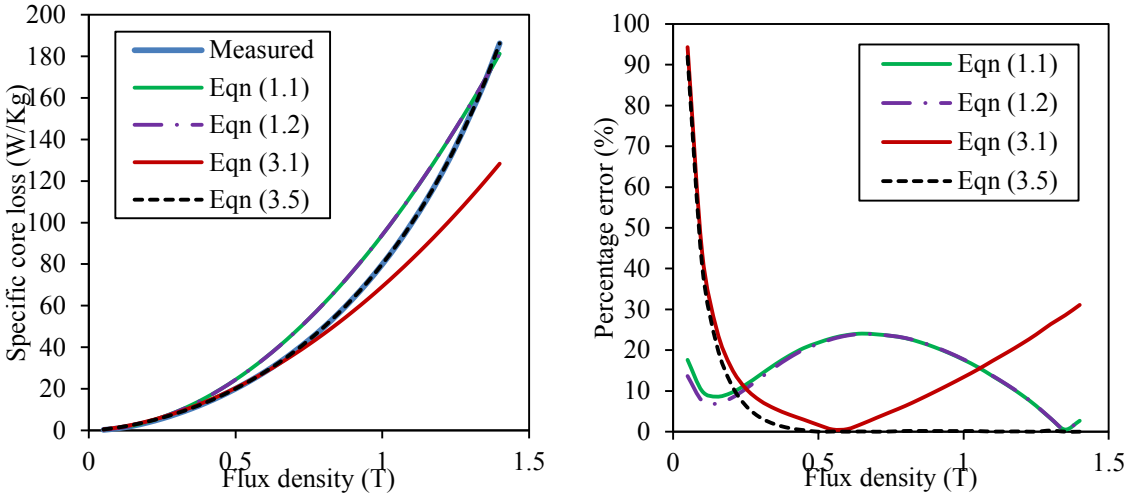

Fig 3.4 Specific core loss and percentage error vs flux density for M19G29 at 1kHz.

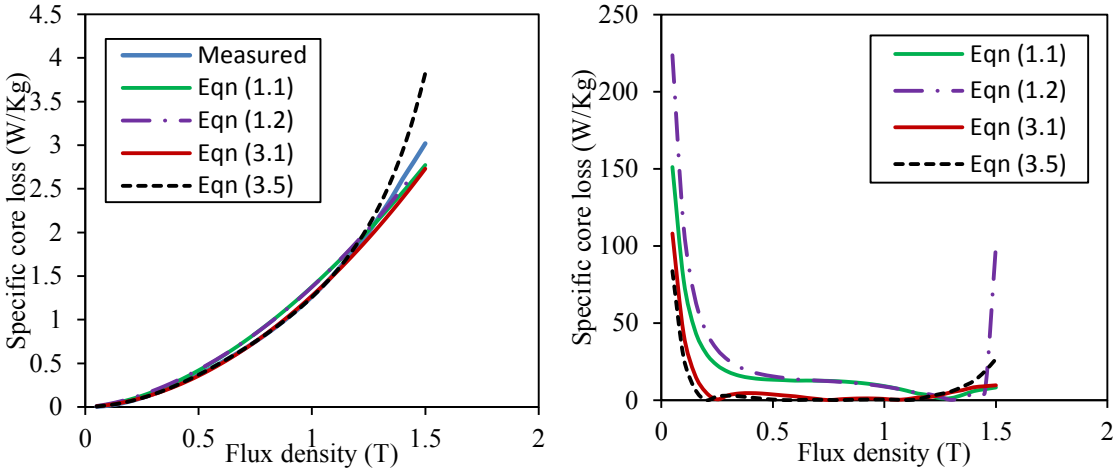

Fig 3.5 Specific core loss and percentage error vs flux density for M36G24 at 60Hz.

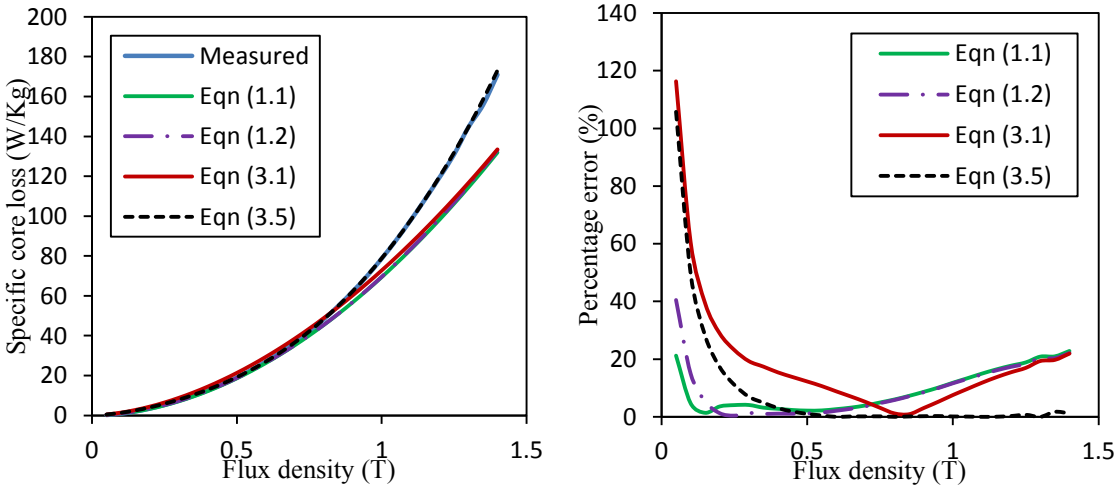

Fig 3.6 Specific core loss and percentage error vs flux density for M36G24 at 1 kHz.

Figs 3.2, 3.4 and 3.6 show the performance of the models at high frequency indicating a general improvement in the prediction compared to the results at 60Hz in Figs 3.1, 3.3 and 3.5. This could be attributed to the fact that at higher frequency less data is available (up to 1.3 or 1.4T) and because all the coefficients used are dependent on the value of B chosen for their calculation. This value is usually above 1T therefore the less the flux density range (up to 1.4T) the more accurate the coefficients hence the better the prediction. Another reason is because the coefficients calculated are average values used for the entire frequency range. Therefore at low frequencies (60Hz) the coefficients are over estimated and at high frequencies (1 kHz) they are closer to the real values hence resulting in a better prediction of the losses.

Generally (3.5) and (1.2) showed better prediction than (1.1) and (3.1). Overall (3.5) showed superiority in the loss prediction when compared to other models at both high and low frequencies. This indicated that the core loss model that includes the excess loss component and allows the Steinmetz coefficient to vary as a quadratic function of flux density allowed a better core loss prediction. When compared to experimental values using percentage error calculations, this model showed some inconsistencies at both low and high flux density. This was evident at both low and high frequencies, with the percentage error even higher at 1 kHz. This was mainly because the algorithm was not suitable for higher frequencies and a wide range of flux density. It assumed constant values for Ke and Ka hence overestimated the loss at low flux density values at each frequency.

In [23] model (3.8) was proposed which was a modification of (3.5), the authors also presented a new algorithm for that model.

$$P_c = P_h + P_e + P_a$$
$$= K_h f B^{(\propto_0 + \propto_1 B + \propto_2 B^2 + \propto_3 B^3)} + K_e f^2 B^2 + K_a f^{1.5} B^{1.5} \quad (3.8)$$

The Steinmetz coefficients $\propto = (\propto_0 + \propto_1 B + \propto_2 B^2 + \propto_3 B^3)$ is a cubic function of flux density and $\propto_0, \propto_1, \propto_2$ and $\propto_3$ are constants. To calculate core losses using this model, a quadratic fit of the specific core loss per cycle (3.9) against square root of frequency is made.

$$P_c/f = a + b(f^{0.5})^2 + cf^{0.5}$$
$$= K_h B^{\propto} + K_e B^2 (f^{0.5})^2 + K_a B^{1.5} f^{0.5} \quad (3.9)$$

Where $a = K_h B^{\propto}$ $b = K_e B^2$and c $= K_a B^{1.5}$. K_e and K_a can be calculated for all values of flux density and fitted to a polynomial of order 3 of the form (3.10) and (3.11).

$$K_a = K_{a0} + K_{a1} B + K_{a2} B^2 + K_{a3} B^3 \quad (3.10)$$

$$K_e = K_{e0} + K_{e1} B + K_{e2} B^2 + K_{e3} B^3 \quad (3.11)$$

The hysteresis loss per cycle "a" can then be obtained after substituting values of b and c using (3.10) and (3.11) for all values of B in (3.9). A plot of Log a verses flux density, as in Fig 3.7, is then made to identify intervals of flux density inflexion on the curve for example B<0.7, 0.7<B<1.4, B>1.4

$$Log\ a = Log\ K_h + (\propto_0 + \propto_1 B + \propto_2 B^2 + \propto_3 B^3) Log\ B \quad (3.12)$$

For a particular frequency for each of the intervals, α and K_h can then be calculated from (3.12) by linear regression using at least five values of B. With all the coefficients K_e, K_a, K_h and α known, the total core loss value can then be obtained from (3.8). This model

however could not be extended to frequencies above 400Hz because of the large variation between the calculated and the measured loss.

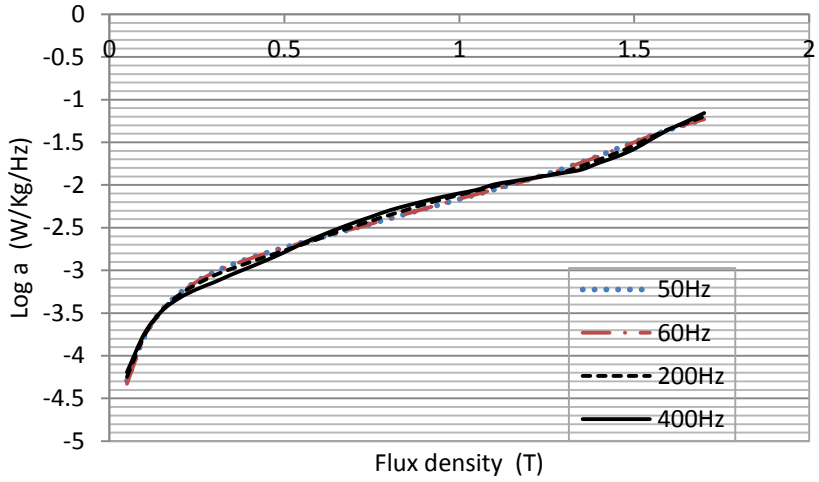

Fig 3.7 Log a vs flux density plot using (3.12) at different frequencies for M19G24.

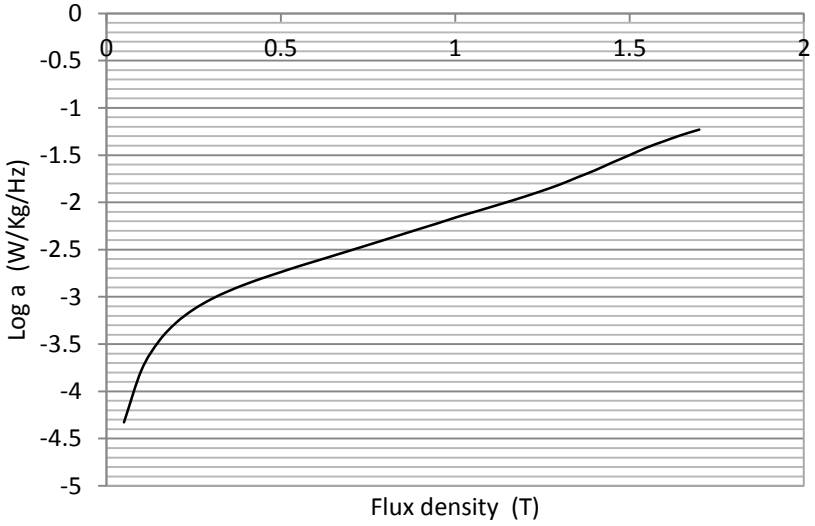

Fig 3.8 Log a vs flux density plot using (3.13) model at 60Hz for M19G24.

(3.8) produced good low frequency results especially when compared to the measured results with an error less than 5%. For increased frequency range above 400Hz to 2 kHz the same authors developed the VARCO and CAL2 models. In [24] these models were presented VARCO (3.13) and CAL2 (3.14).

$$W_{Fe} = K_h f B^{\propto} + K_e f^2 B^2 \quad (3.13)$$

$$W_{Fe} = K_h(f,B) f B^2 + K_e(f,B) f^2 B^2 \quad (3.14)$$

The algorithm used for (3.13) is the same as that of (3.8) except that the coefficients were determined by linear fitting instead of quadratic fitting and the data is divided into low frequency range (60-400Hz), medium range (400Hz – 1kHz) and high frequency range (above 1kHz) before calculation.

(3.13) also gave good results over a wide range of frequency and flux densities although because of the complexity and length of its algorithm, CAL2 model was suggested.

To calculate core losses using the CAL2 model, (3.14) is divided through by B^2 *and* f yielding the linear equation (3.15).

$$\frac{W_{Fe}}{fB^2} = K_h(f,B) + K_e(f,B) f \quad (3.15)$$

where K_e and K_h can be determined graphically since plotting $\frac{W_{Fe}}{fB^2}$ vs f gives a straight line whose slope is K_e and K_h is the y-intercept. The calculated coefficients are fitted to (3.11) and (3.16) to calculate the eddy current and hysteresis losses respectively.

$$K_h = K_{h0} + K_{h1} B + K_{h2} B^2 + K_{h3} B^3 \quad (3.16)$$

The total core loss at each flux density is then calculated using (3.14) with the hysteresis and eddy current coefficients known. In general K_e, K_a, K_h were functions of B therefore enabling their calculation at any value of B. This model was the simplest model to implement although it gave the highest percentage error when compared to the other models proposed by the same authors. Fig 3.9-Fig 3.11 show the percentage error when (3.8), VARCO and CAL2 are used for core loss prediction respectively.

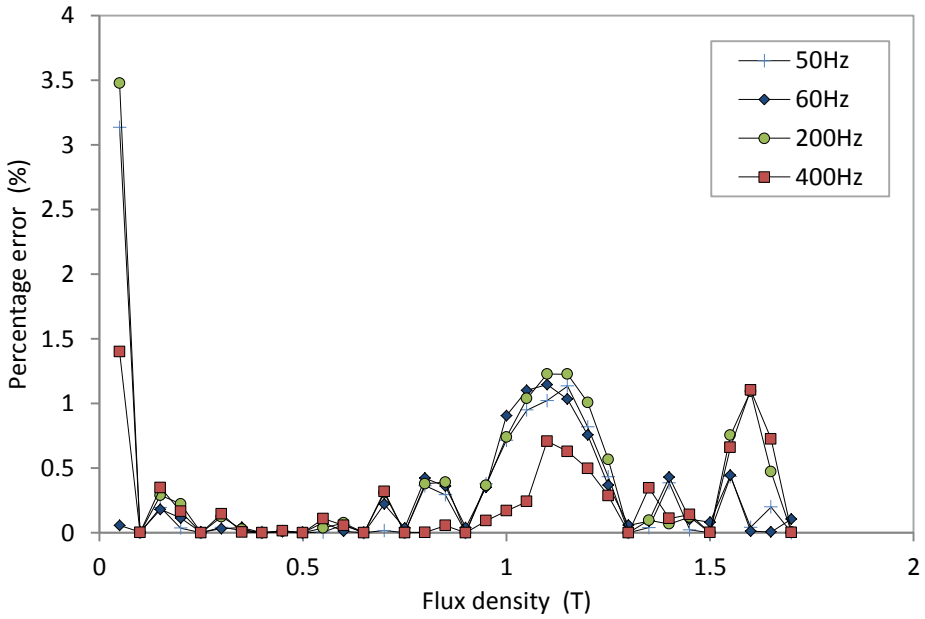

Fig 3.9 Percentage error vs flux density for M19G24 using (3.8).

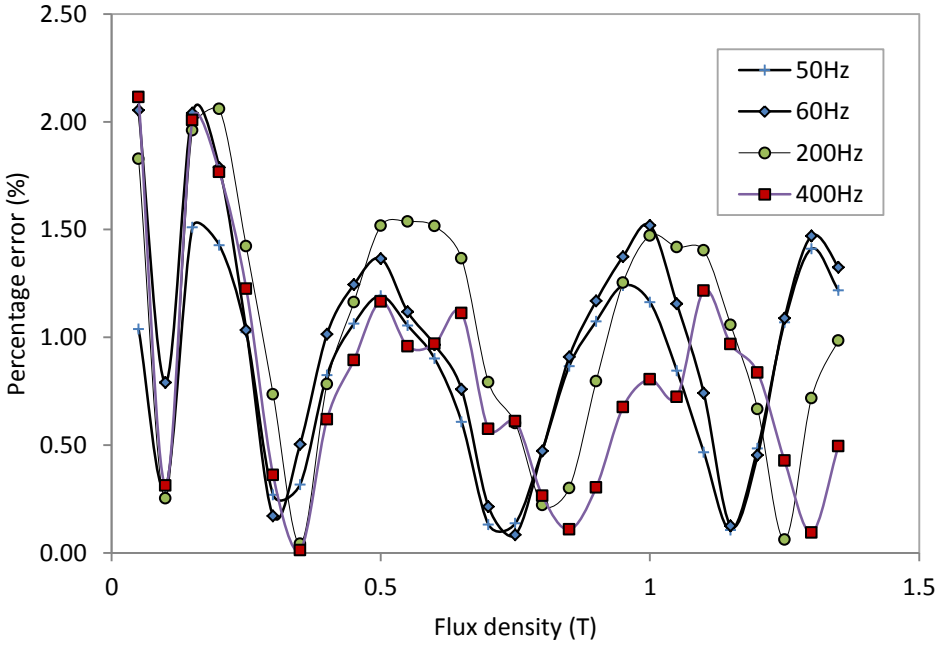

Fig 3.10 Percentage error vs flux density for M19G24 using the VARCO model.

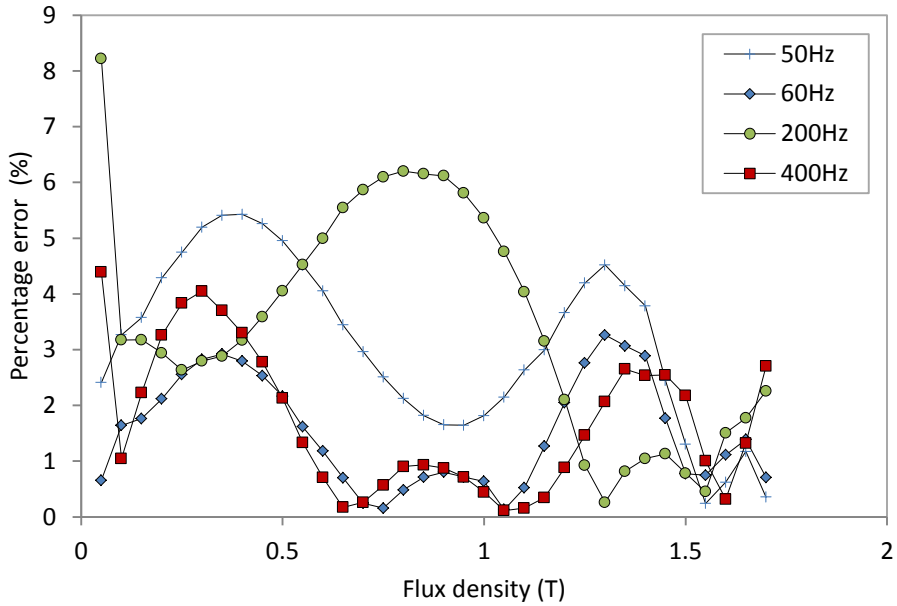

Fig 3.11 Percentage error vs flux density for M19G24 using CAL2 model.

It can be seen that generally (3.8) gave good approximations of the measured loss at different frequencies in the range of 0-1.5% except for one point which is 3.5%. The VARCO when compared to the measured loss gave an error in the range of 0 – 2.2% while the CAL2 gave an error in the range of 0 -6.3%with a maximum error of 8.1%. These maximum errors found out of range especially for the first point could be attributed to computational errors or error in the reading of the first data point.

Fig 3.12 shows the comparison of (3.8), VARCO (3.13) and CAL2 (3.14) for M19G24 material at 60Hz. In general all the models accurately predicted core loss within acceptable errors and of the three models (3.8) was the most accurate followed by the VARCO model then CAL2. However as previously mentioned, (3.8) could not be extended to frequencies above 400Hz, VARCO had a complex algorithm and CAL2 gave the highest deviation from the measured values when the three models where considered.

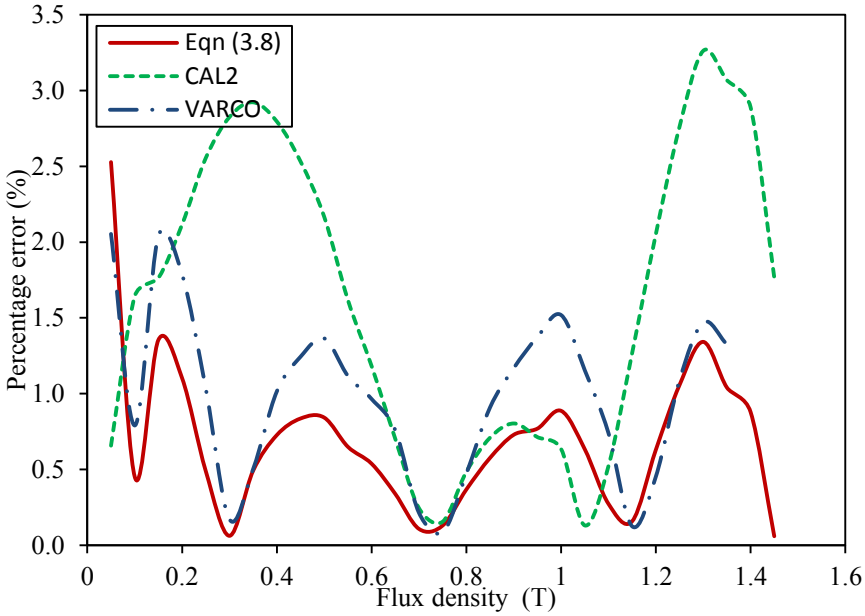

Fig 3.12 Comparison of (3.8), CAL2 and VARCO at 60Hz for M19G24.

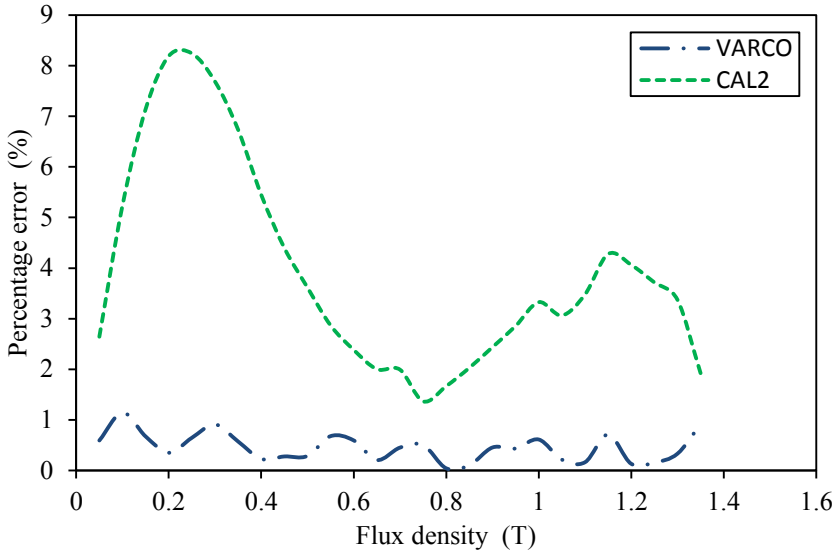

Fig 3.13 Comparison of the VARCO and CAL2 models at 1 kHz for M19G24.

The CAL2 model was an easier algorithm to implement that could be extended to higher frequencies and required less experimental data for evaluation. For good results, the frequencies had to be divided into a low frequency range (50Hz-400Hz) and high frequency range from (400Hz-1 kHz) and for each range the same procedure followed.

Since Model (3.8) could not be extended to frequencies above 400Hz, Fig 3.13 only shows a comparison of CAL2 and VARCO at 1 kHz with VARCO being more accurate.

3.2 Proposed model

In order to maintain a somewhat simple algorithm with a good approximation of core loss and a wide range of frequency up to 4kHz and flux density up to 1.7T, a new algorithm referred to as model M is proposed based on (3.5).

$$\begin{aligned} P_c &= P_h + P_e + P_a \\ &= K_h f B^{(a+b B+c B^2)} + K_e f^2 B^2 + K_a f^{1.5} B^{1.5} \end{aligned} \tag{3.17}$$

- The total core loss is divided through by frequency $\frac{P_c}{f} = K_h B^{(a+bB+cB^2)} + K_e f B^2 + K_a f^{0.5} B^{1.5}$
- This gives an equation of the form $\frac{P_c}{f} = D + E\left(f^{0.5}\right)^2 + G f^{0.5}$ where $D = K_h B^{(a+bB+cB^2)}$ $\mathrm{E} = \mathrm{K_e B^2}$ and $\mathrm{G} = \mathrm{K_a B^{1.5}}$
- Plot $\frac{P_c}{f}$ vs $\sqrt{f}$ for all values of B and make a quadratic fit for each value of flux density.
- Calculate K_e and K_a from G and E and plot K_e and K_a vs B as shown in Fig 3.14 and Fig 3.15 using M15G29 that gave the lowest R-squared values among all the material used.
- Make a fit of a 3rd order polynomial for both curves of the form

$$\begin{aligned} K_a &= K_{a0} + K_{a1} B + K_{a2} B^2 + K_{a3} B^3 \\ K_e &= K_{e0} + K_{e1} B + K_{e2} B^2 + K_{e3} B^3 \end{aligned} \tag{3.18}$$

- Calculate P_h from $P_h = P_c - P_e - P_a$ substituting K_e and K_a for all values of B.
- Using at least eight or all values of flux density a, b, c and K_h can be calculated from $\log P_h = \log f + \log K_h + \left(a + bB + cB^2\right)\log B$

for a given frequency. With all the coefficients known the total core loss can then be calculated from (3.5).

The fitting of Ka and Ke to 3rd order polynomials in B enables the calculation of these coefficients at any value of B, this finds application in a machine flux waveform where the flux density may not be a round figure or a fixed value as in measured data. The method of loss separation also allows for unique values of specific hysteresis loss per cycle for each flux density instead of using one value for the whole flux density range as in (1.1), (1.2), (3.1) and (3.5).

In comparison to (3.5), the new model uses actual values for the coefficients instead of the average values for the whole range of flux density. This goes a long way not to overestimate losses at low frequencies and underestimate losses at high frequencies. Because both models are best fit models using more data points to calculate the hysteresis coefficient and the Steinmetz coefficients improves the accuracy of the model.

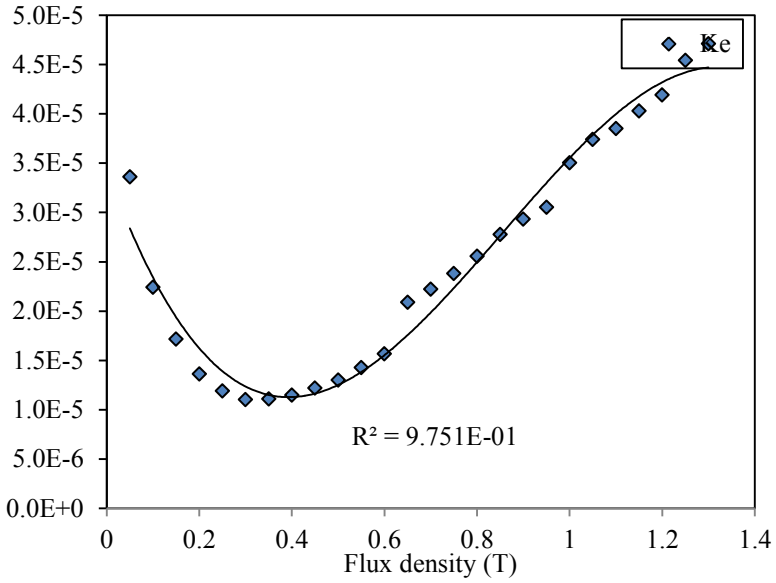

Fig 3.14 Plot of the K_e coefficient vs flux density for M15G29

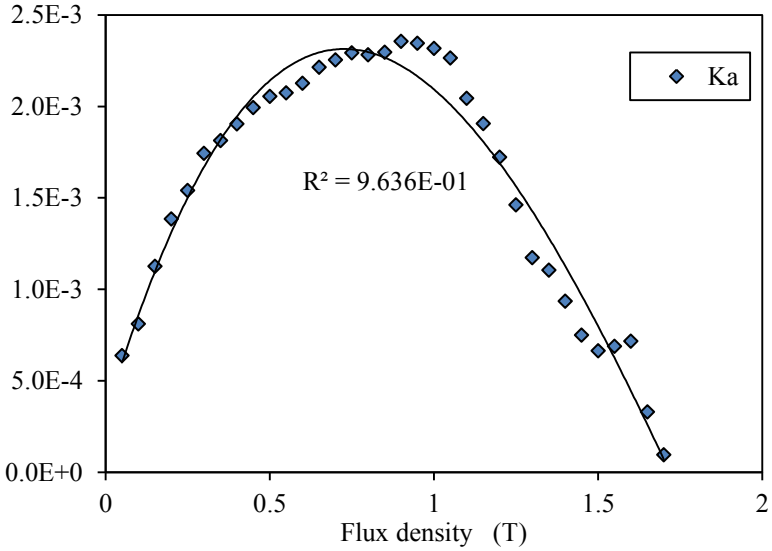

Fig 3.15 Plot of the K_a coefficient vs flux density for M15G29.

Improving these areas in the algorithm enabled it to be used for high frequency and high flux density core loss calculations while accurately predicting losses even at low flux densities. Fig 3.16 shows that the percentage error using the proposed model is less than 6% at low frequencies. The calculated core loss when compared to the measured core loss at high frequencies as in Fig 3.17, also showed a good correlation.

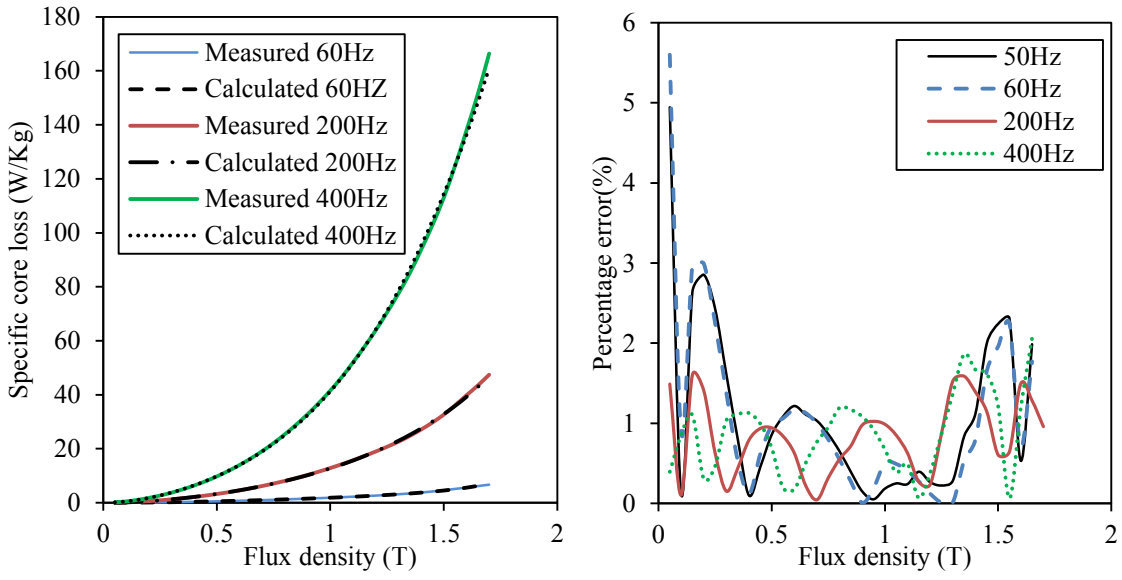

Fig 3.16 Low frequency core loss calculations using model M for M19G24.

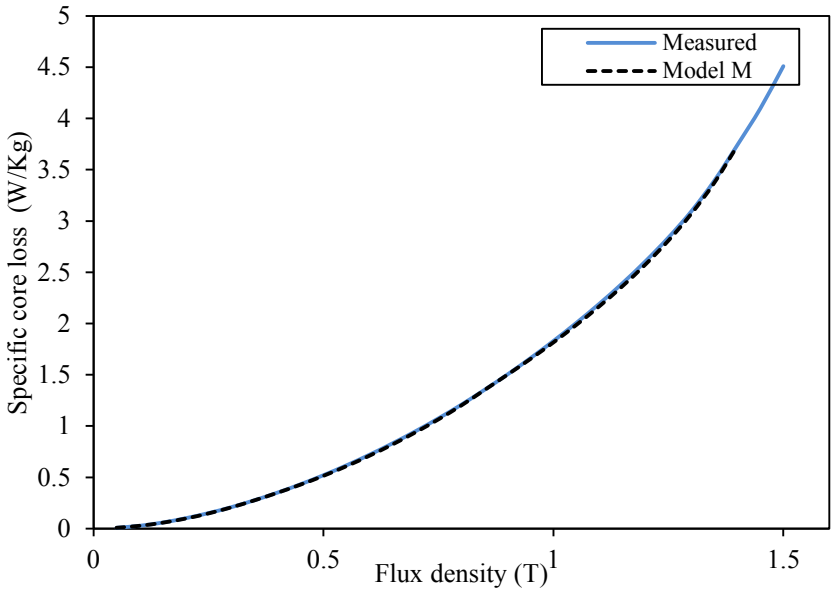

Fig 3.17 Core loss calculations using Model M at 60Hz for M19G24.

To validate this model, the results obtained are compared to (3.8), VARCO and CAL2 as shown in Fig 3.18. Model M gave errors within the range of 0-3% comparable to (3.8) and the VARCO model yet it had a simpler algorithm and could be extended to frequencies above 400Hz.

The rest of the comparison using different materials will only be done using the CAL2 model since the authors who developed CAL2 along with the other models have subsequently focused on CAL2 in their subsequent papers [24] [25]. Figs 3.18-3.20 show the comparison of this model with CAL2 using different materials at 60Hz and 1 kHz. Overall the two models can be compared with model M performing better at higher frequencies in some materials and CAL2 at lower frequency in other materials.

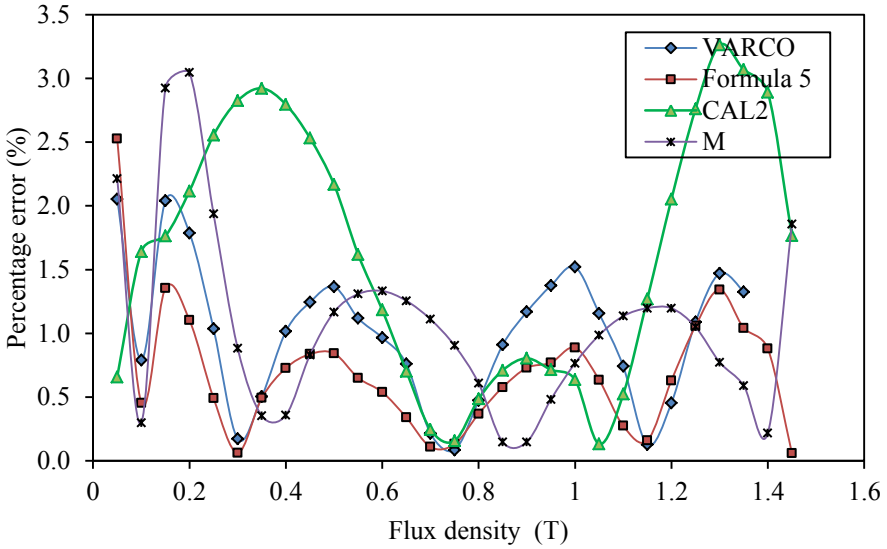

Fig 3.18 Comparison of the models using M19G24 at 60Hz.

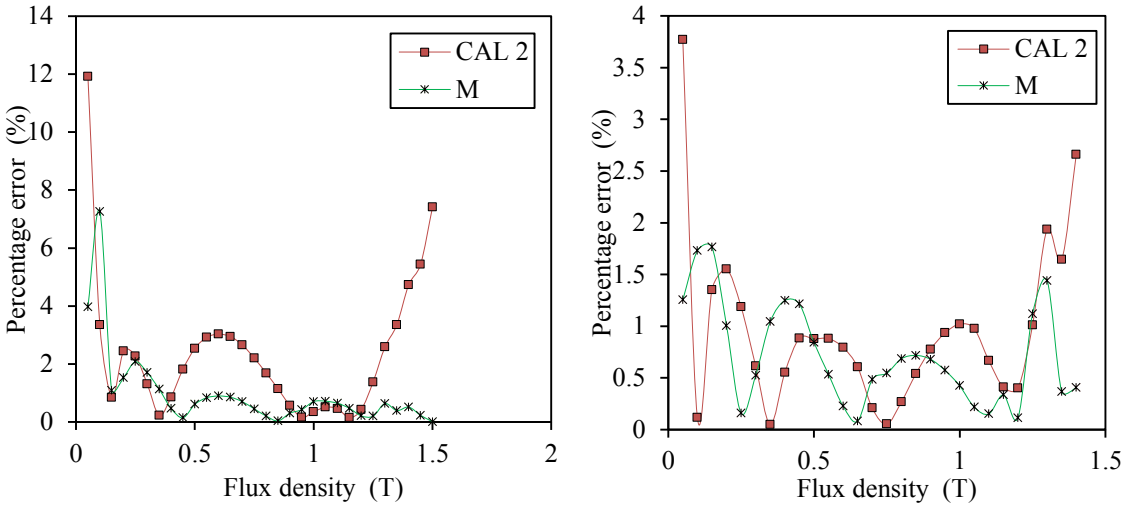

Fig 3.19 Percentage error vs flux density for 60Hz and 1 kHz respectively using M15G29.

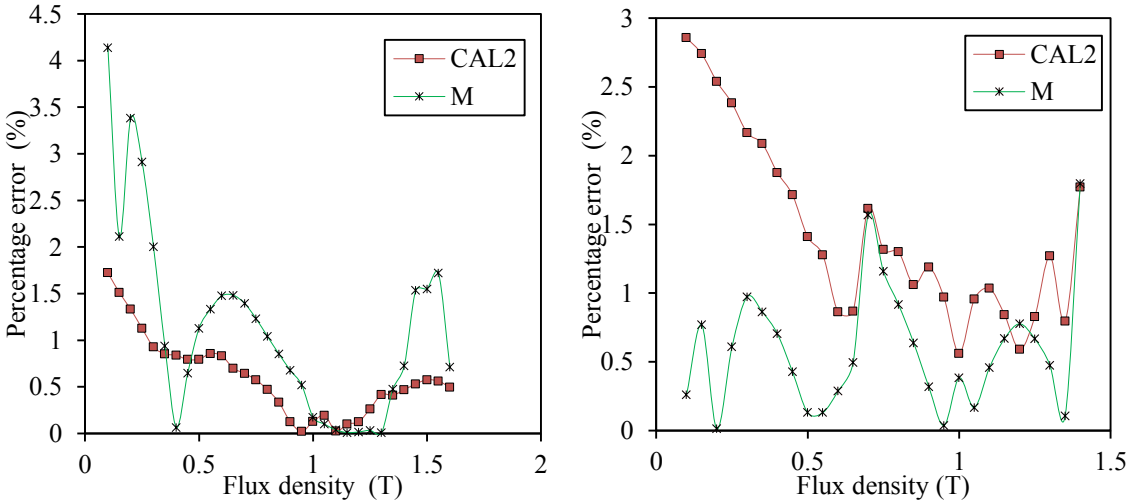

Fig 3.20 Percentage error vs flux density for 60Hz and 1 kHz respectively using M36G24

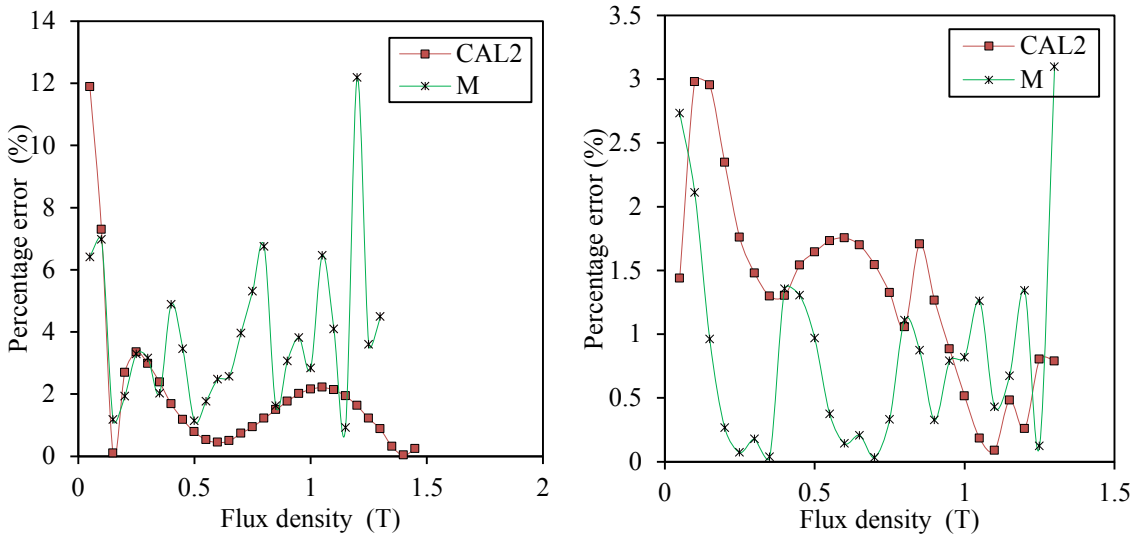

Fig 3.21 Percentage error vs flux density for 60Hz and 1000Hz respectively using M45G26

3.3 Comparison with Model M

The models above were compared on the assumption that quadratic and linear fits are comparable irrespective of their individual assumptions, limitations and advantages over each other. Fig 3.22 shows the linear and quadratic fitting where the linear fit is used by models with three loss terms and linear fitting used by models with only two loss terms.

Although each of the models gives a good approximation of the total core losses, accuracy varies depending on the model and all the models seem to follow certain trends when the percentage error is calculated.

- At lower values of flux density the errors are higher
- The absolute error across all values of B is not a constant value but is within a certain range.

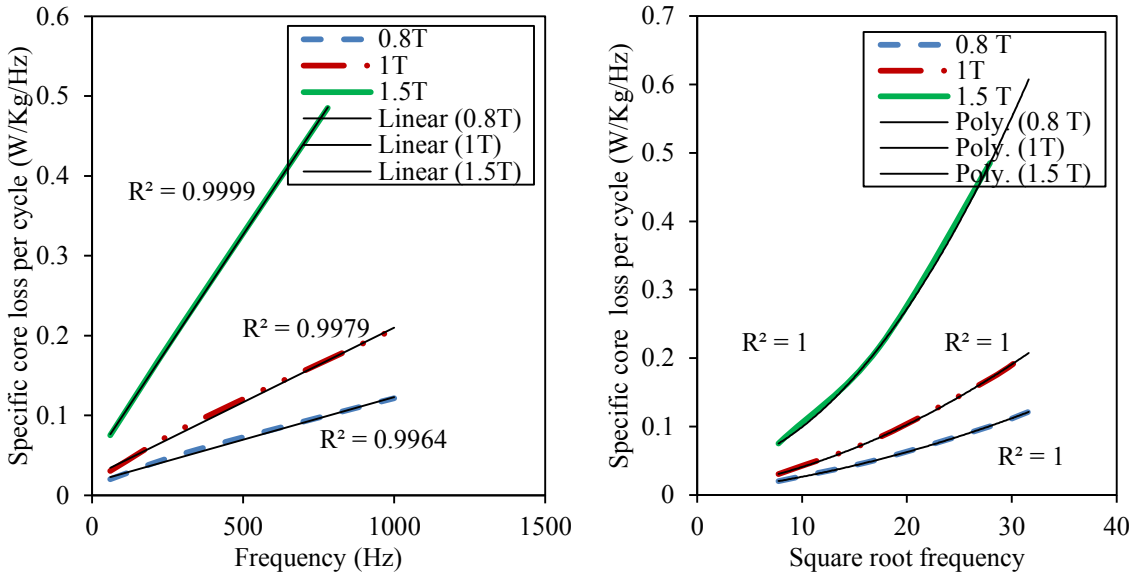

Fig 3.22 Linear and quadratic fitting used on the models for M19G24.

The range of prediction also varies for the different models in terms of the frequency range and the flux density range. Some models for example (3.8) are limited to frequencies below 400Hz although it allows for a wide range of flux density from 0.05T-2T while CAL2 and model M allow for wider frequency ranges up to 1 kHz or 4 kHz their range of flux density is limited to 1.5T or less depending on the available data.

Another important factor considered when comparing the different models is the complexity of the algorithm. Some models use linear fitting while others use quadratic fitting for example models (1.1), (3.1), CAL2 and VARCO use linear fits while models (1.2), (3.5) and model M use quadratic fits.

Table 3-1 Qualitative comparison of the M, CAL2, VARCO and (3.8) models.

Model	**Eqn (3.8)**	**VARCO**	**CAL2**	**M formula**
Formula components	$P_h+P_e+P_a$	P_h+P_e	P_h+P_e	$P_h+P_e+P_a$
Frequency Range	Low range (0-400Hz)	Low range (0-400Hz) Medium range (400-1kHz) High range (above 1kHz)	Low range (0-400Hz) Medium range (400-1kHz) High range (above 1kHz)	Low range (0-400Hz) Medium range (400-1kHz) High range (above 1kHz)
Percentage error	0-5%	0-5%	0-12%	0-12%
Algorithm	Complex	Complex	Somewhat simple	somewhat simple

Other processes in the algorithm like the fitting of Ke and Ka into a polynomial, plotting of log "a", dividing the flux densities into intervals, calculation of the coefficients using all the data points or most of the data points make some models more tedious and complex therefore requiring additional calculation time and memory space for computation. Table 3.1 shows a summary of the comparison of the last four models.

Model M could also be extended to high frequencies up to 4 kHz. Fig 3.23 and Fig 3.24 show these results for M45G26 and M15G29 materials.

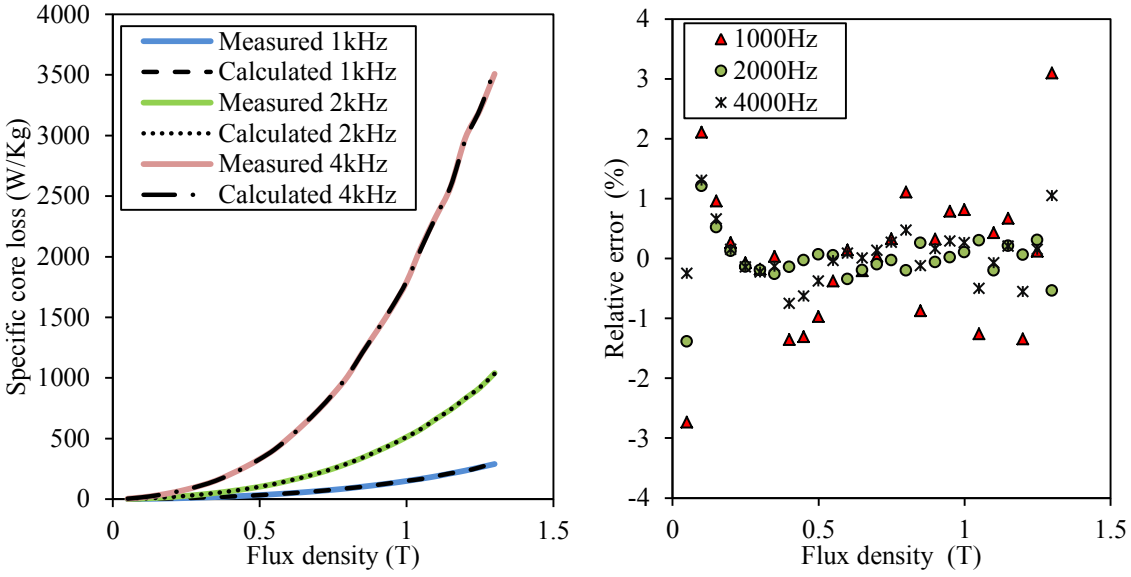

Fig 3.23 Plots of model M at high frequencies for M45G26

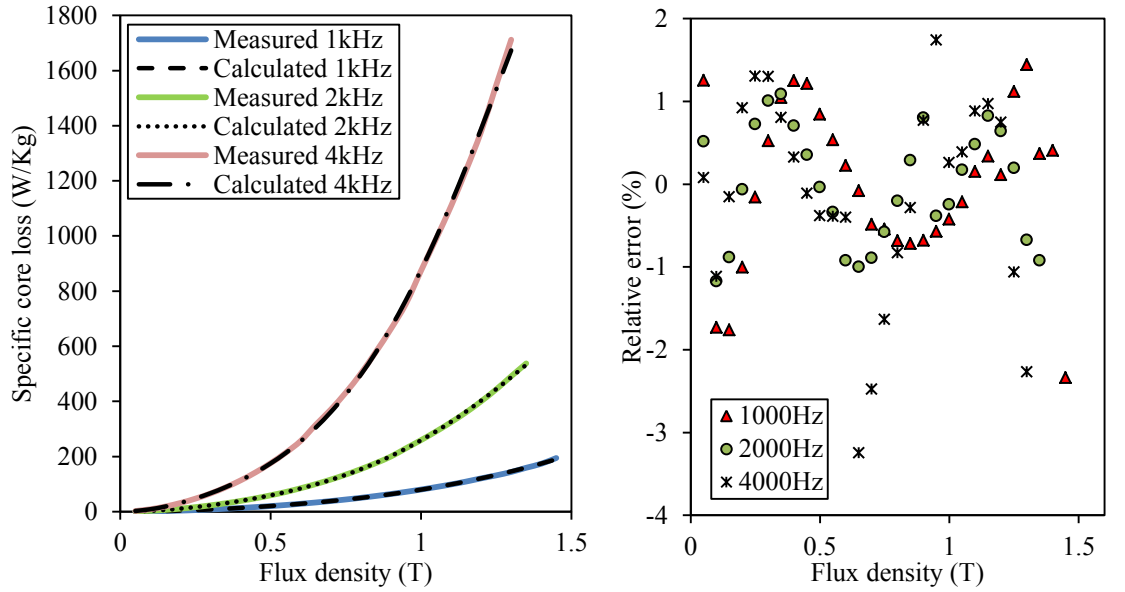

Fig 3.24 Plots of model M at high frequencies for M15G29

3.4 Summary

Although different methods for core loss prediction exist, to choose which model to use, a designer (machine or software designer) has to make tradeoffs between the accuracy, robustness and complexity of the algorithm depending on their need.

In this chapter different methods of core loss prediction have been presented and an algorithm proposed for an already existing model to allow for core loss prediction over a wide frequency and flux density range. Results obtained after testing this algorithm were also presented for different steel types across different frequency and flux density ranges showing acceptable errors.

Chapter 4 Core loss Coefficients

All the models presented in chapter 3 use the extrapolation method to calculate the hysteresis loss per cycle. This method of loss separation is obtained from the assumption that flux density distribution is uniform across the lamination thickness which is true only at low frequencies (<400Hz) or even 200Hz in other materials. This method of loss separation although has found a lot of application in core loss calculations [22] [24] [25] [26] [27] does not take into account any physical characteristics occurring in the material. Because these are purely best fit models using curve fitting techniques, they each have their limitations for example frequency range, flux density range, material limitations and they all require a wide range of data at different frequencies and flux densities to calculate the total losses. These models cannot be extended to data out of the range for which they are applied. Attempts to extend them to other data gave large errors. One of the reasons behind most of these limitations is mainly because these models do not include physical characteristics occurring in the material. Methods that include the physical characteristics or behavior of the field in the material require the analytical solution of Maxwell's equations. Since the method of loss separation used in a model also affects the models results therefore reflecting on the accuracy of the formula used, a better separation method is required.

4.1 Loss separation

Calculating the hysteresis loss per cycle from the total losses by extrapolation involves extrapolating the specific loss per cycle to zero frequency for all values of flux density. This value of the hysteresis loss obtained is only accurate for lower frequencies however

when the frequency increases and skin effect occurs in the material this method then under-estimates the value of hysteresis loss hence causing a discrepancy between the measured values and the calculated losses. This is also evident by addition of the excess current loss term in the core loss formulas to meet the difference between the calculated and the measured loss. This term can work well mathematically in some cases as in (3.5), (3.8), some authors [28] split this term into a hysteresis component and an eddy current loss component while other authors argue that this term doesn't exist since it cannot be physically separated from the eddy current loss, its effect is included in the eddy current component [4] [29].

In [30] a method of loss separation is developed based on the fact that the effective flux density at a point in the lamination thickness is different from the flux density at the boundary of the lamination especially at high frequencies. The analytical model developed calculates the flux density at the boundary, divides the lamination into sections small enough to assume the flux distribution in those sections is uniform. The flux density in each of those sections y distance from the center is calculated using (4.1) from which the loss can be obtained.

$$B_p(\hat{y}) = B_b \sqrt{\frac{\cosh\left(\frac{2\hat{y}}{\lambda}\right) + \cos\left(\frac{2\hat{y}}{\lambda}\right)}{\cosh\left(\frac{2}{\lambda}\right) + \cos\left(\frac{2}{\lambda}\right)}} \tag{4.1}$$

$$\lambda = \sqrt{\frac{2}{L^2 \omega \mu \sigma}} \tag{4.2}$$

Where $\hat{y} = \frac{y}{L}$, L, B_p, B_b, μ, σ, ω are half the lamination thickness, flux density at a point, flux density at the boundary, magnetic permeability, electrical conductivity and

angular frequency respectively. The total hysteresis loss is therefore the summation of the loss from each of the sections. Once obtained, the eddy current loss can then be calculated from (4.3).

$$P_e = P_c - P_h \tag{4.3}$$

Where P_e, P_c, P_h are the eddy current loss, total core loss and the hysteresis loss respectively. This separation method was applied on loss data obtained from different testers; Epstein tester, single sheet tester and toroid tester to show the difference between the hysteresis loss per cycle obtained by this model and by extrapolation. Figs 4.1-4.3 show the loss separation for the different testers using M19G24 material data.

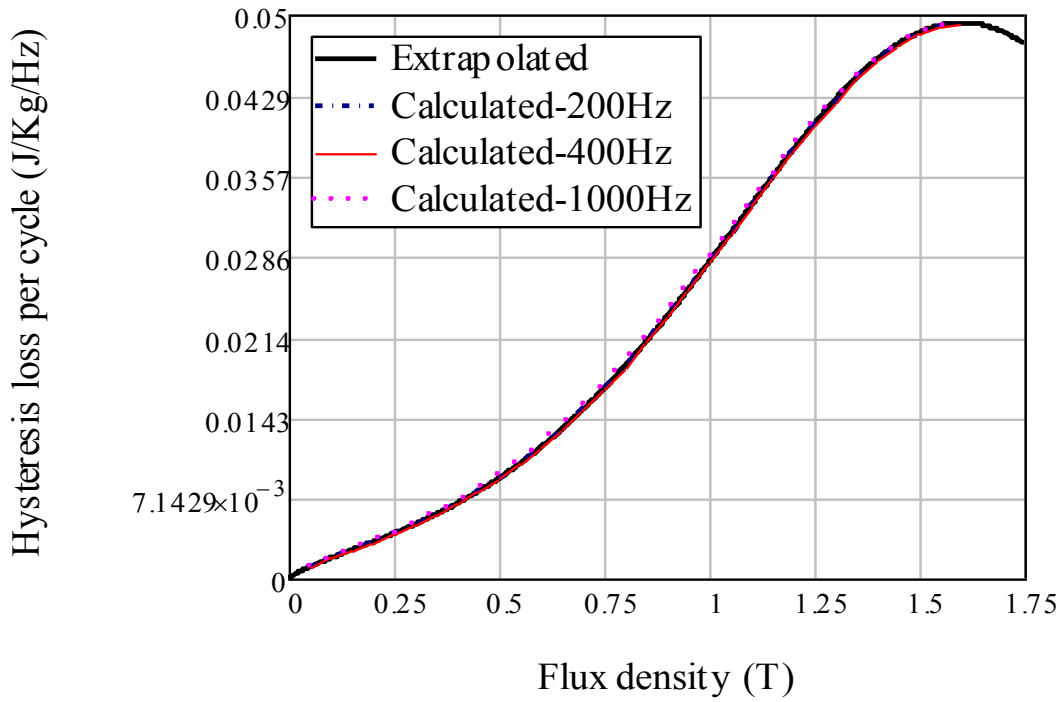

Fig 4.1 Comparison of the separation at different frequencies with the toroid tester for M19G24.

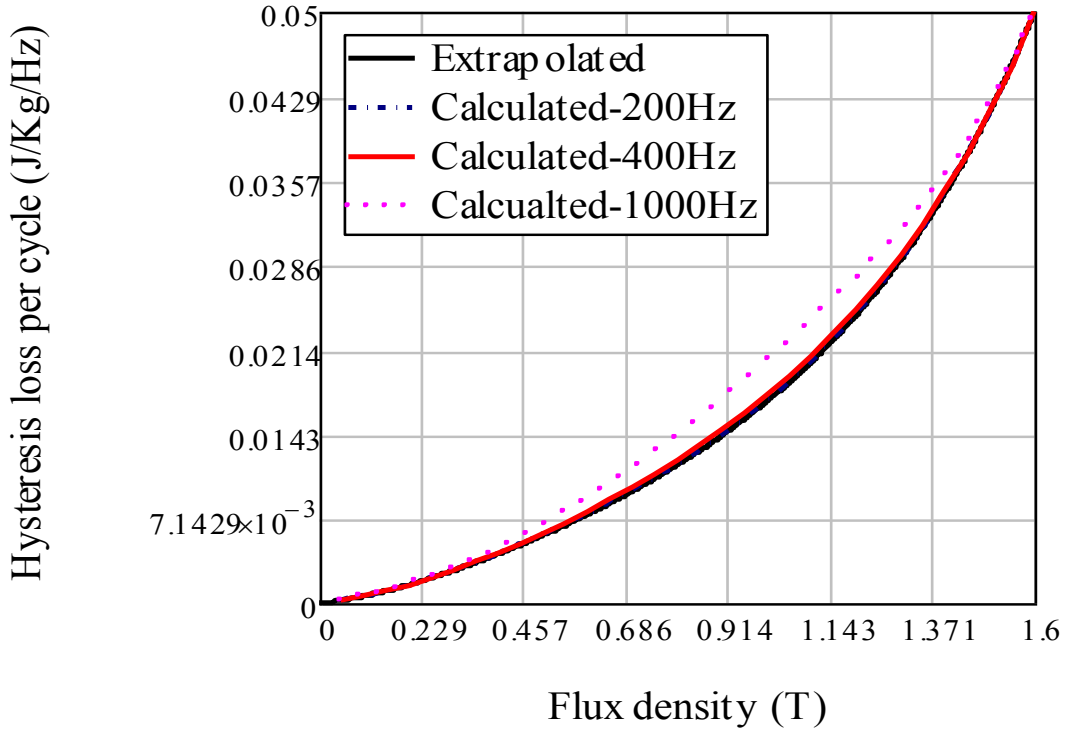

Fig 4.2 Comparison of the separation at different frequencies with the SST tester for M19G24.

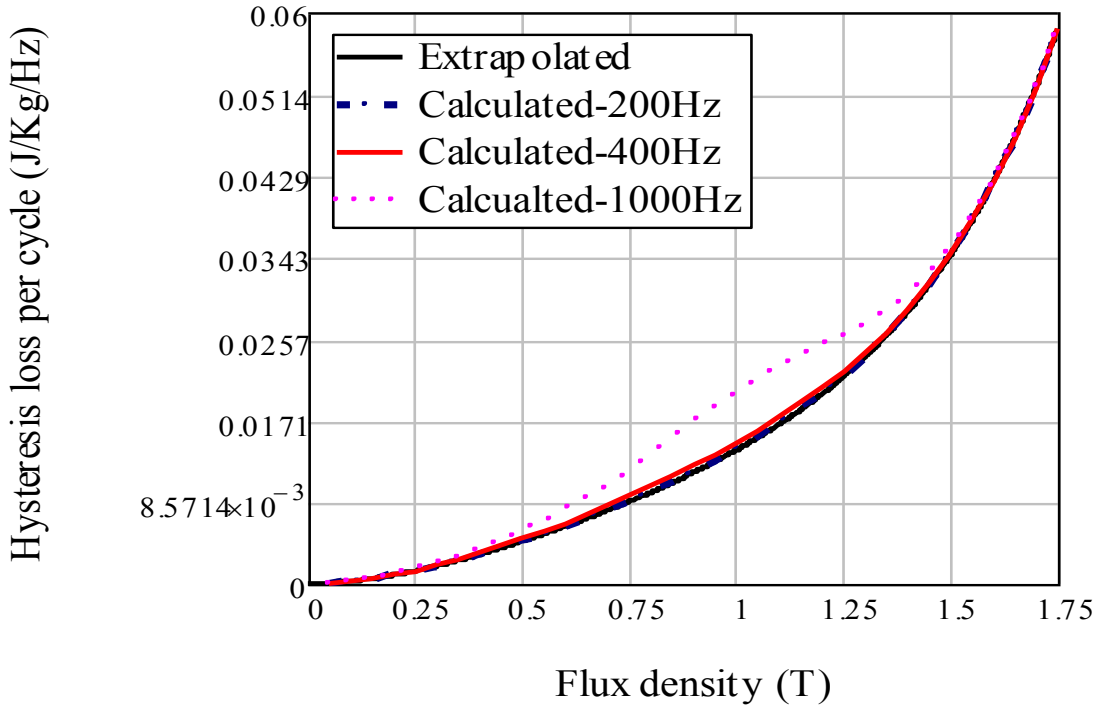

Fig 4.3 Comparison of the separation at different frequencies with the Esptein tester for M19G24.

In all the testers from the figures above, at low frequencies (below 400Hz) there is a small difference if any between the hysteresis loss per cycle obtained using both methods. However as the frequency increases above 400Hz, this difference becomes more visible as expected because of skin effect. The toroid tester however shows no difference even at higher frequencies. This is mainly because the toroid sample experiences shearing stress reflected in the core loss and permeability results. Also because it has very small dimensions, it is not a very good reflection of the material.

Since most of the data used for core loss calculations is based on experimental data obtained from Epstein measurements, the results above express a need to incorporate better loss separation methods in the core loss formulas. Based on this method of separation, core loss only consists of the hysteresis loss and the eddy current loss.

The method of separation when applied separates the total loss into the hysteresis loss and the eddy current loss therefore applying this separation to a two term core loss model can give us an insight on the behavior of the coefficients. The two term models used were the Steinmetz equation and its derivative.

4.2 Fitting to equations

4.2.1 Steinmetz Equation

From the results obtained with the new method of separation, using (1.1) the hysteresis component is fitted to the calculated hysteresis loss and the eddy current component is fitted to the calculated eddy current component.

As shown in [25] the coefficient K_e varies with flux density and also with frequency therefore for a given value of frequency K_e is obtained for each value of flux density B

using (4.4), K_h and n using (4.5) by linear regression.

$$K_e = \frac{P_e}{f^2 B^2} \tag{4.4}$$

$$\log P_h = \log K_h + n \log B \tag{4.5}$$

The coefficients obtained were then used to calculate the losses and a comparison made with the measured losses. This was done for four types of materials; M19G24, M45G26, M36G24 and M15G29.

Figs. 4.4-4.7 show the comparison between the calculated loss obtained by using coefficients K_h and n and the loss obtained from the new separation method. Some materials like M15G29 and M19G24 showed a good correlation between the measured and calculated loss for the three frequencies tested. However M36G24 and M45G26 gave a variation in results with a percentage error of up to 40% especially at higher frequencies of 400Hz and 1 kHz. It is worth noting that even with the large variation in the calculated and measured loss, the calculated loss is very close to the measured loss especially for flux density below 1T. This result is true for the Steinmetz equation however to have an equation that sufficiently calculates core loss over a wide frequency and flux density range, the Steinmetz equation needs to be modified accordingly.

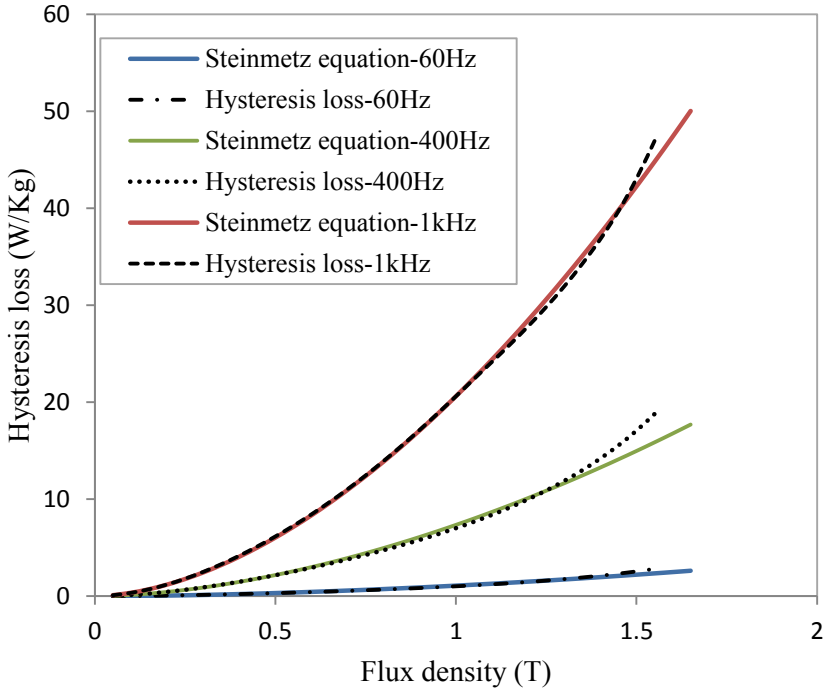

Fig 4.4 Comparison of the hysteresis component using Steinmetz equation with M15G29

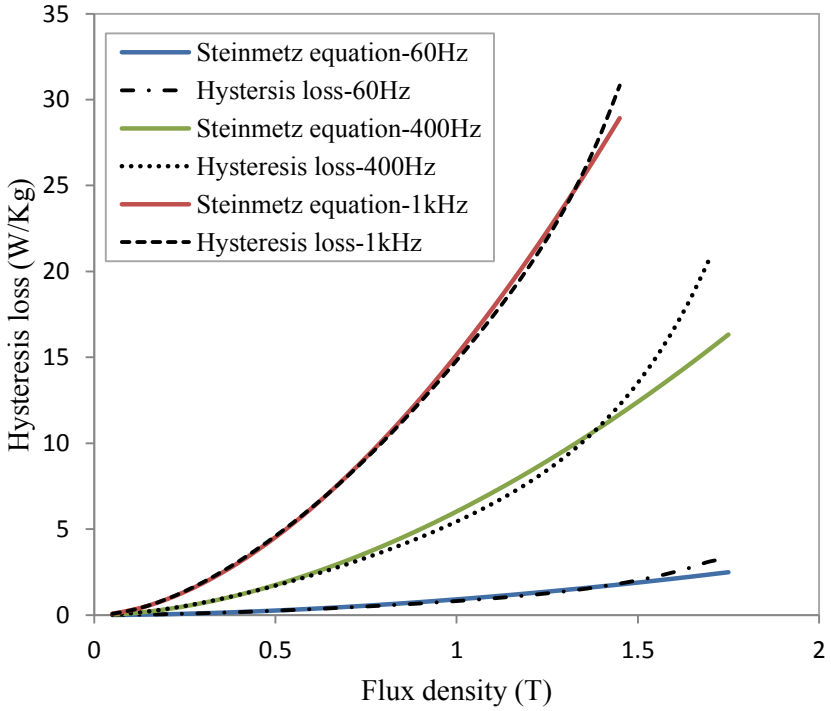

Fig 4.5 Comparison of the hysteresis component using Steinmetz equation with M19G29

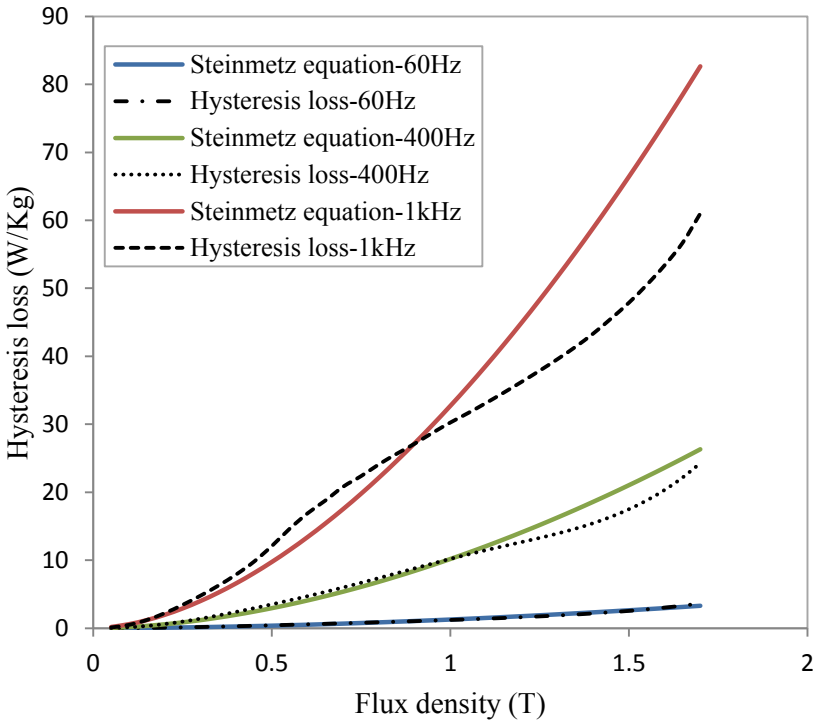

Fig 4.6 Comparison of the hysteresis loss component using Steinmetz equation with M36G24

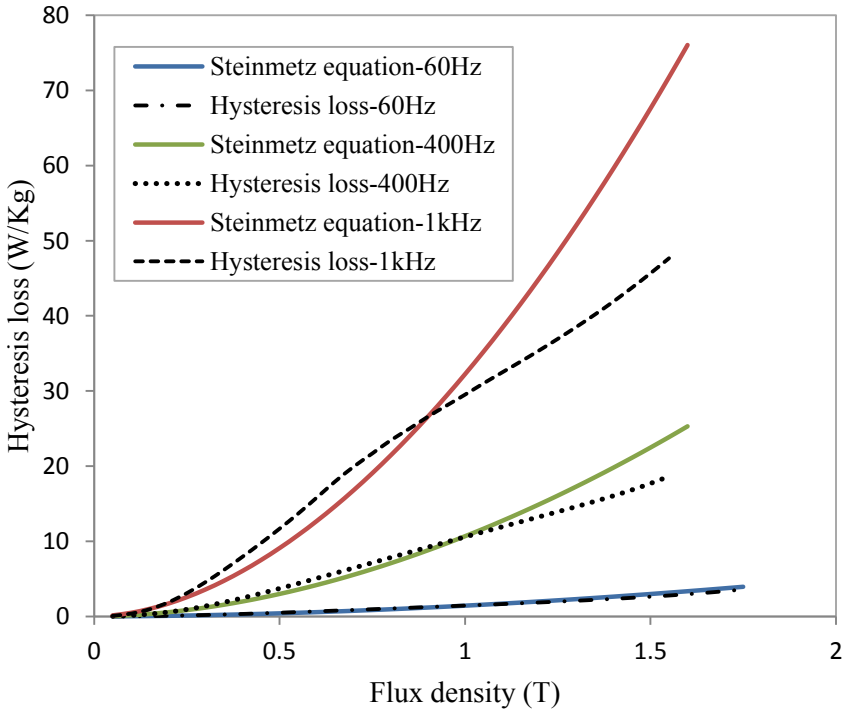

Fig 4.7 Comparison of the hysteresis loss component using Steinmetz equation with M45G26

In general these results indicate that the model is more suited for some materials than others in this case low grade materials M19 and M15. The Steinmetz coefficients should be dependent on flux density rather than being a constant value.

4.2.2 Modified Steinmetz

In [22] [31] reference is made to various modifications of the Steinmetz equation for better prediction of losses. One of the modifications is to allow the Steinmetz coefficient to vary with flux density as in the M formula. Again the separated losses are fitted to the hysteresis and eddy current components respectively using (4.6).

$$P_c = P_h + P_e = K_h f B^{(a+b B+cB^2)} + K_e f^2 B^2 \quad (4.6)$$

Where a, b and c are constant coefficients for a given frequency. K_e is calculated from (4.4), K_h, a, b and c are determined from (4.7) by linear regression.

$$\log P_h = \log K_h + \log f + (a + bB + cB^2) \log B \quad (4.7)$$

Using the obtained coefficients, the hysteresis loss is calculated and the results compared with the measured losses. Figs 4.8-4.11 show the comparison of the two losses for different materials at different frequencies. The results indicate a good correlation between the measured and calculated loss for all the materials and frequencies tested hence the importance of allowing variable coefficients.

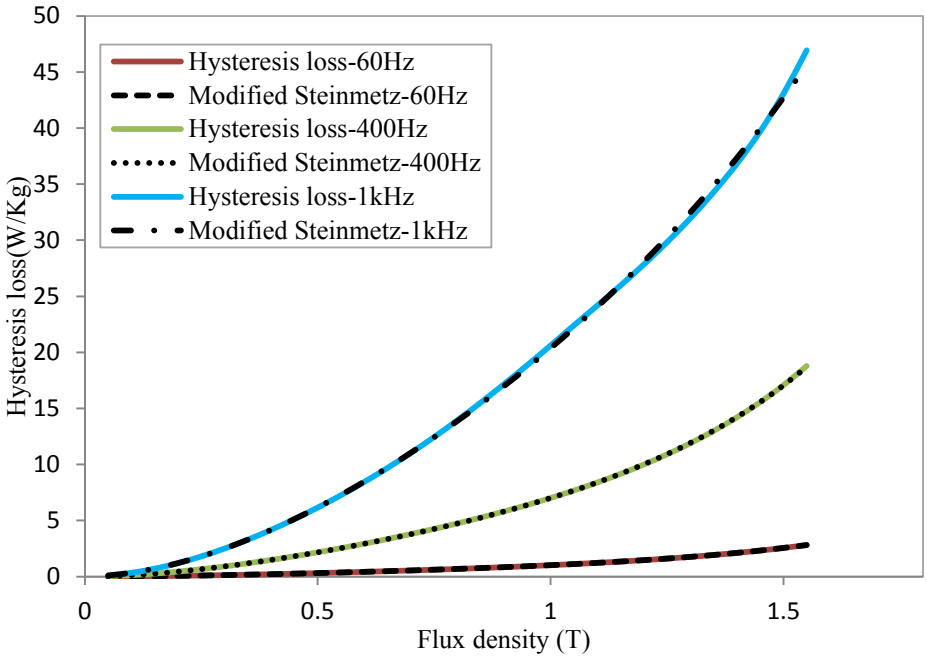

Fig 4.8 Comparison of the hysteresis component using modified Steinmetz equation with M15G29

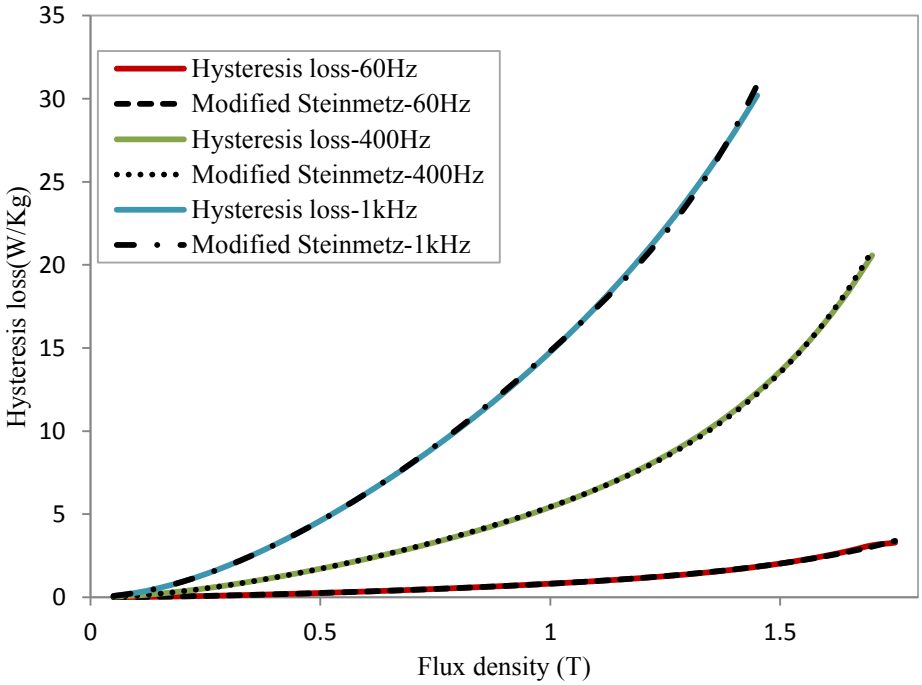

Fig 4.9 Comparison of the hysteresis component using modified Steinmetz equation with M19G24

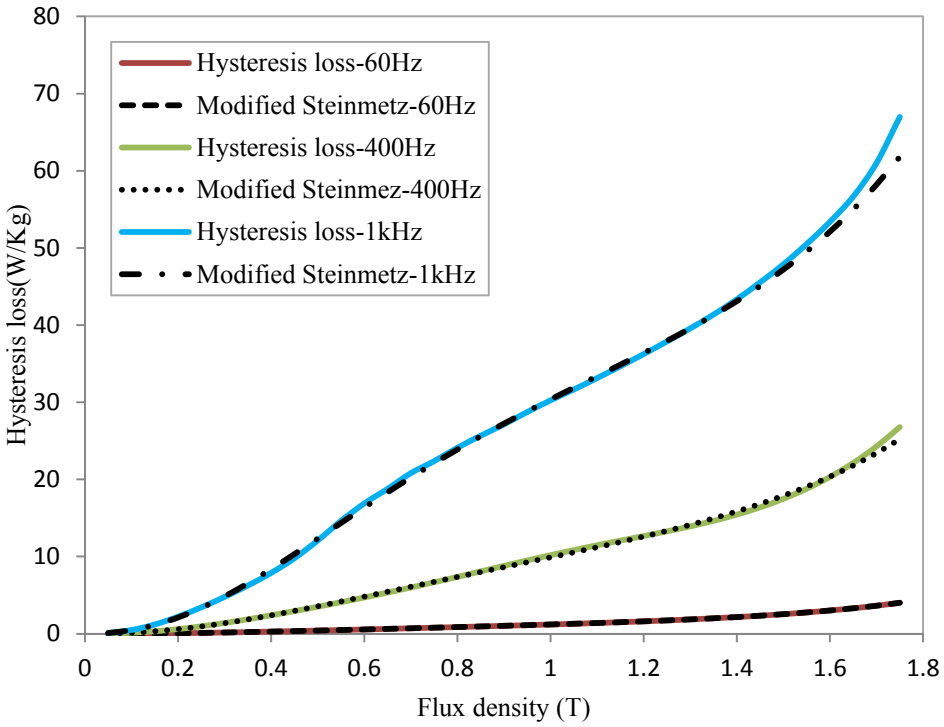

Fig 4.10 Comparison of the hysteresis component using modified Steinmetz equation with M36G24

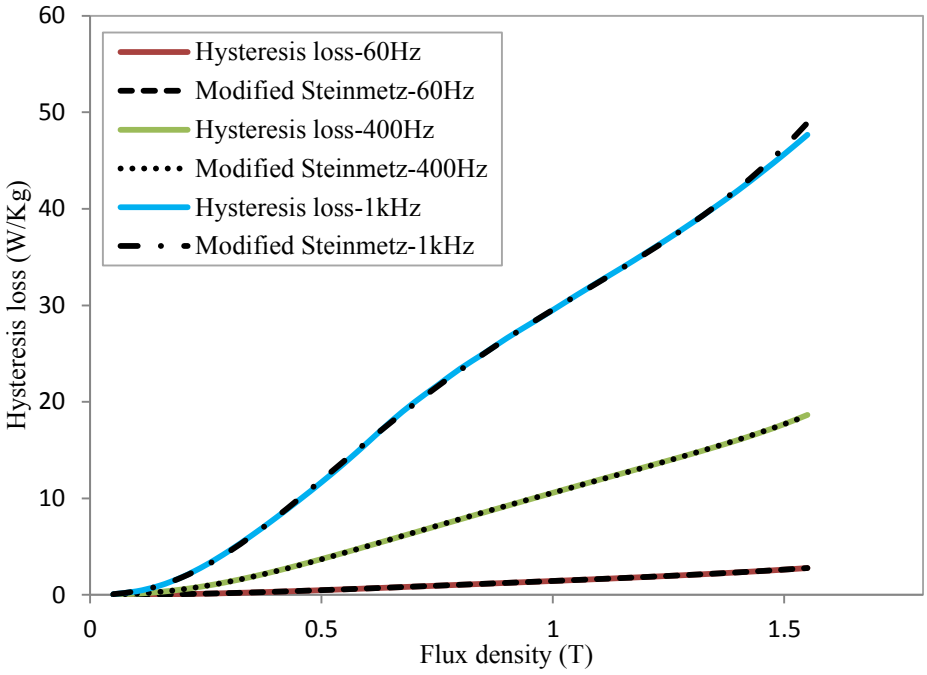

Fig 4.11 Comparison of the hysteresis component using modified Steinmetz equation with M45G26

The coefficients obtained for K_h, a, b, c for the different materials at different frequencies are shown in Table 4.1.

Table 4-1 Hysteresis and Steinmetz coefficients at different frequencies

M36G24				
Frequency (Hz)	**60**	**200**	**400**	**1000**
K_h	0.020114072	0.02118849	0.024757113	0.030373861
a	1.9389	1.9537	1.9915	1.9734
b	-1.1837	-1.3107	-1.3793	-1.724
c	0.7447	0.7761	0.6834	0.7554
M15G29				
K_h	0.016998085	0.017127738	0.017518624	0.020370421
a	1.744	1.7496	1.757	1.7955
b	-0.317	-0.3321	-0.3372	-0.2297
c	0.443	0.4429	0.4182	0.1666
M45G26				
K_h	0.023999379	0.024711551	0.026448436	0.029546089
a	2.014	2.0219	2.0512	2.085
b	-1.185	-1.2151	-1.3362	-1.9967
c	0.551	0.5366	0.543	0.899
M19G24				
K_h	0.013592521	0.013635	0.013555015	0.014760464
a	1.747	1.758	1.7484	1.7633
b	-0.413	-0.445	-0.4394	-0.3133
c	0.4978	0.5068	0.5231	0.2937

For frequencies below 400Hz, K_h is almost the same for each of the materials and generally increases at higher frequencies. All higher grade and all lower grade materials each have about the same coefficient values for example the value of K_h for M36 and M45 are close for the different frequencies and those for M15 and M19 are also similar. This shows a dependency of the coefficients on the material properties since both the high and low grade materials each exhibit similar properties. Using (4.8) the Steinmetz coefficient for each material is plotted against flux density in the Figs 4.12 – 4.15 below to show its variation at different frequencies.

$$n = (a + bB + cB^2) \tag{4.8}$$

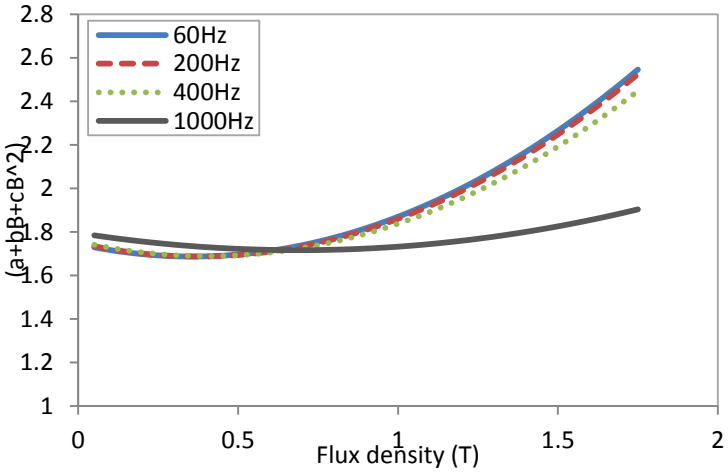

Fig 4.12 Steinmetz coefficient at different frequencies for M15G29

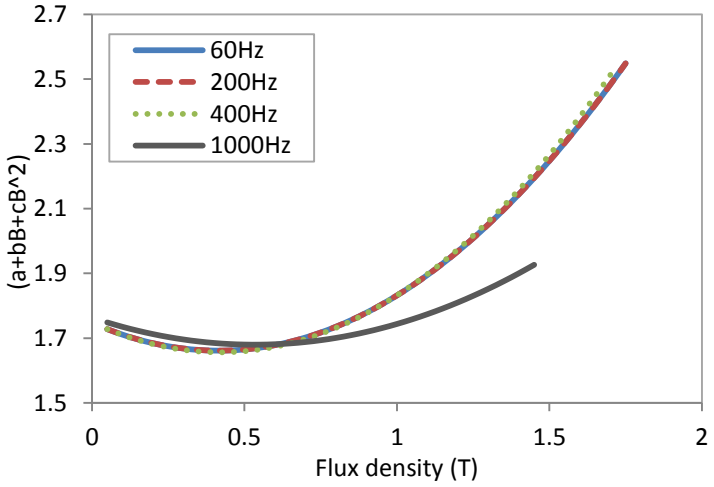

Fig 4.13 Steinmetz coefficient at different frequencies for M19G29

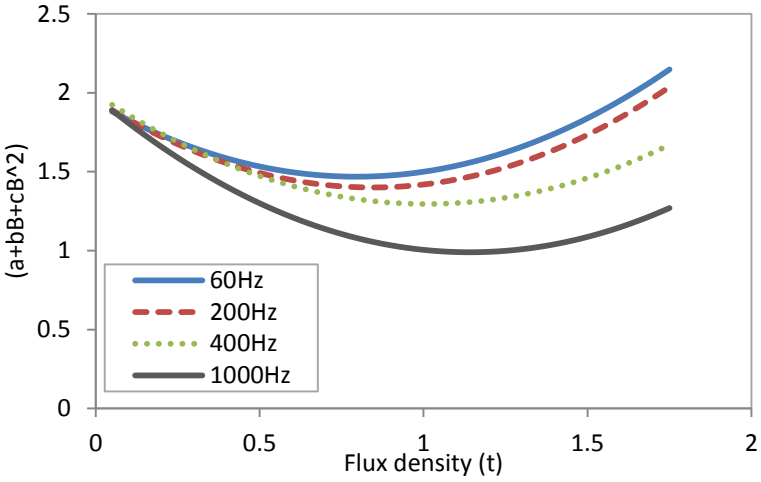

Fig 4.14 Steinmetz coefficient at different frequencies for M36G24

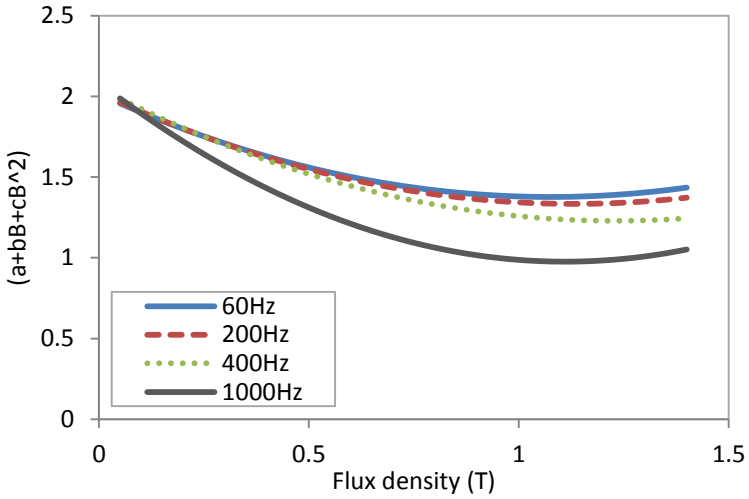

Fig 4.15 Steinmetz coefficient at different frequencies for M45G26

From the figures above, the Steinmetz coefficient n varies with both frequency and flux density. For low grade materials M19 and M15, n is almost the same for all frequencies below 400Hz and it decreases for frequencies above 400Hz. This trend is not true for the M36 and M45 materials whose Steinmetz coefficient is different at each frequency. These differences could be attributed to the material properties being more evident in higher loss materials. n ranges between 1.4 – 1.99 as in table 4.2 which makes models that use constant Steinmetz coefficients 1.6 [3] and 2 [24] correct at least for a certain materials, over a certain range of flux density and frequency.

Table 4-2 Typical Steinmetz Coefficient (n) up to 1.5T

Material	60Hz	200Hz	400Hz	1000Hz
M36G24	1.88-1.83	1.89-1.73	1.92-1.46	1.89-1.08
M15G29	1.73-2.26	1.73-2.25	1.74-2.19	1.78-1.83
M45G26	1.96-1.48	1.96-1.4	1.98-1.27	1.99-1.11
M19G24	1.73-2.25	1.73-2.25	1.73-2.26	1.75-1.95

Because these coefficients vary with both frequency and flux density and also with the type of material, finding a general equation that combines all these factors is not easy therefore the coefficients were defined based on individual properties like their frequency and flux density variation.

Coefficients a, b and c were found to vary with frequency as shown in Figs 4.15-4.18, this relationship is defined in (4.9). Generally for all the coefficients good R-squared values greater than 0.9 were obtained. Fig 4.18 shows that the c coefficient for M36G24 which gave a low R-squared value.

$$a = A_0 + A_1 f + A_2 f^2$$
$$b = N_0 + N_1 f + N_2 f^2 \quad (4.9)$$
$$c = L_0 + L_1 f + L_2 f^2$$

Where A, N and L are constants.

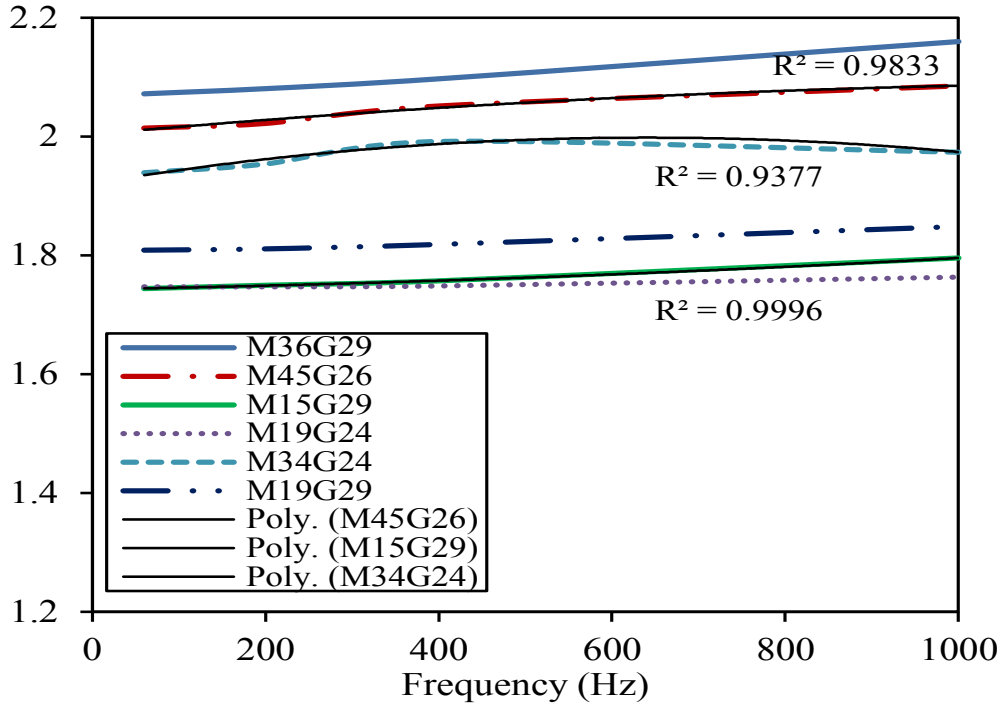

Fig 4.16 Coefficient a vs frequency.

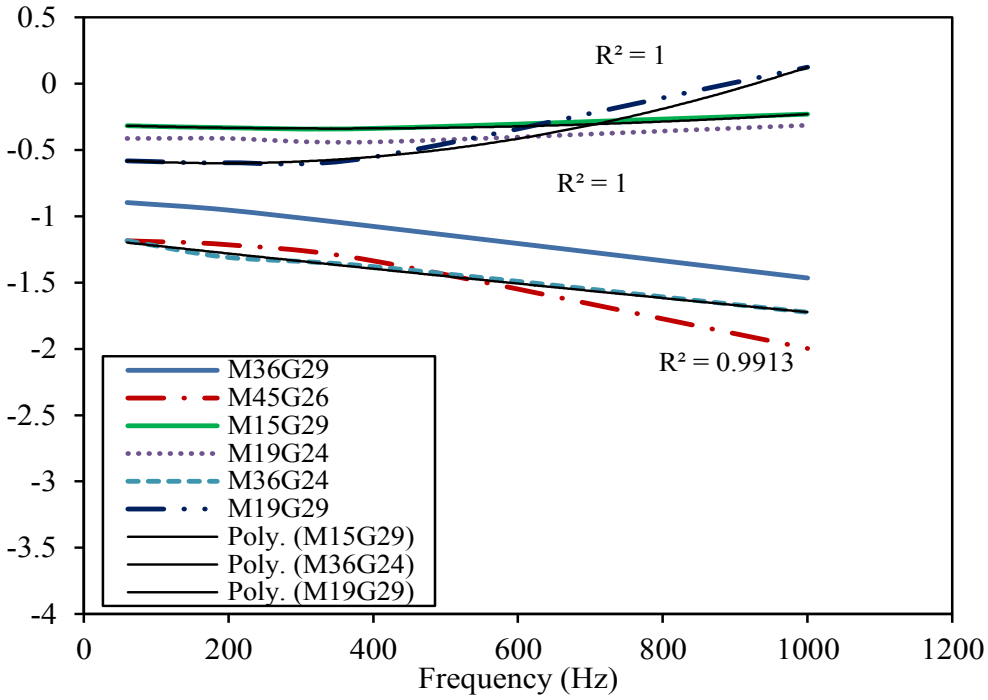

Fig 4.17 Coefficient b vs frequency.

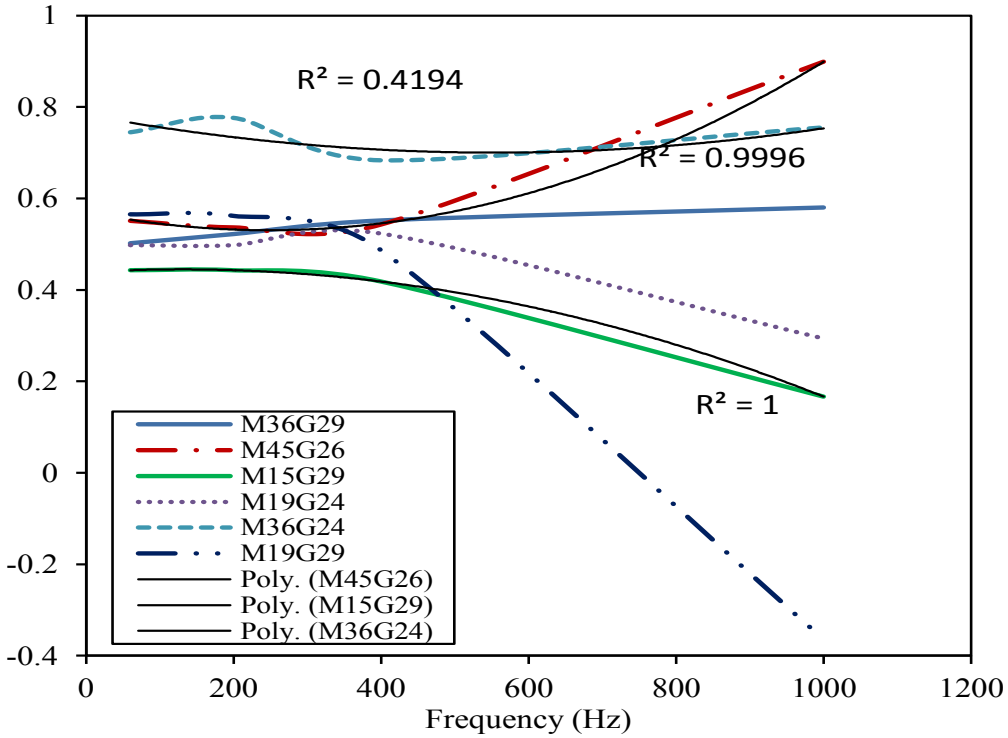

Fig 4.18 Coefficient c vs frequency.

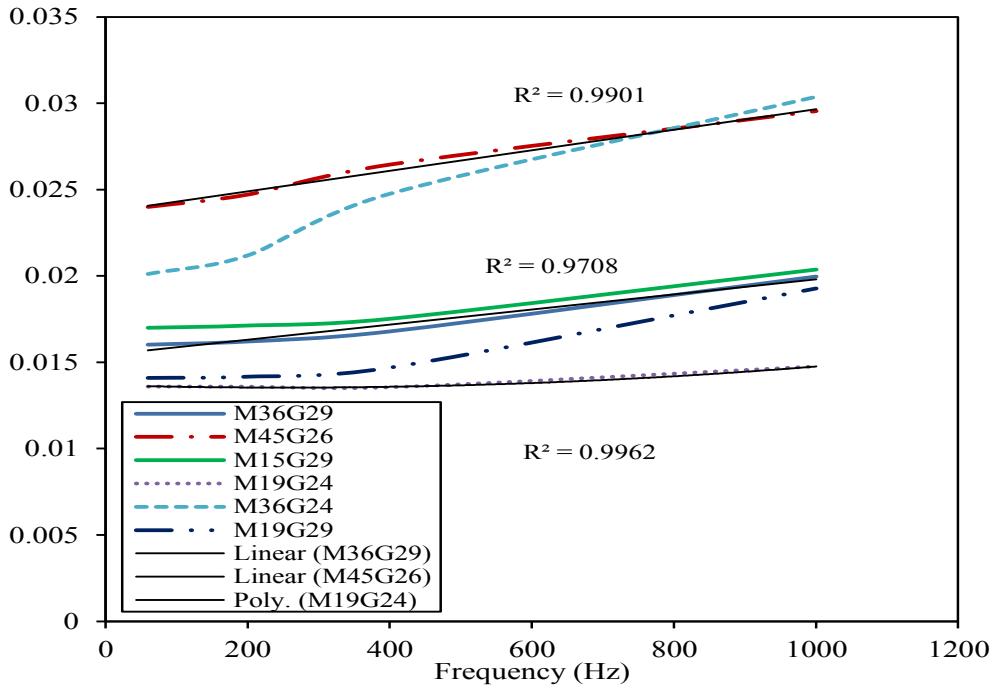

Fig 4.19 Hysteresis coefficient vs frequency.

K_h was found to be almost constant with flux density but varied with frequency as in Fig 4.19 above. The values of K_h were constant especially for frequencies below 400Hz with a linear increase for frequencies above 400Hz. This relationship between the frequency and K_h was found to be linear.

In general the hysteresis loss coefficient and Steinmetz coefficients were therefore found to vary with both frequency and flux density which is consistent with [26].

Since the method for evaluating the eddy current loss is the same for both formulas (1.1) and (4.6) reviewed, the calculated loss obtained was the same for both models with maximum percentage error of 4% when compared to the measured loss. Emphasis is therefore on determining the correlation between the eddy current coefficient with both frequency and flux density. Fig 4.20 - Fig 4.23 show the variation of K_e with both frequency and flux density.

No one function has been obtained yet to show this relationship although functions can be

obtained by looking at its variation with flux density. This coefficient was reported constant dependent on material properties by [32] [33]. However the relationship found was a fourth order polynomial (4.10) in B with good R-squared values as shown in the figures below using different materials therefore indicating a dependence on both frequency and flux density [26] [34]. When an exponential function was used the fitting obtained was not as good.

$$K_e = A_0 + A_1 B + A_2 B^2 + A_3 B^3 + A_4 B^4 \tag{4.10}$$

where A_0, A_1, A_2, A_3, A_4 are constants dependent on the frequency.

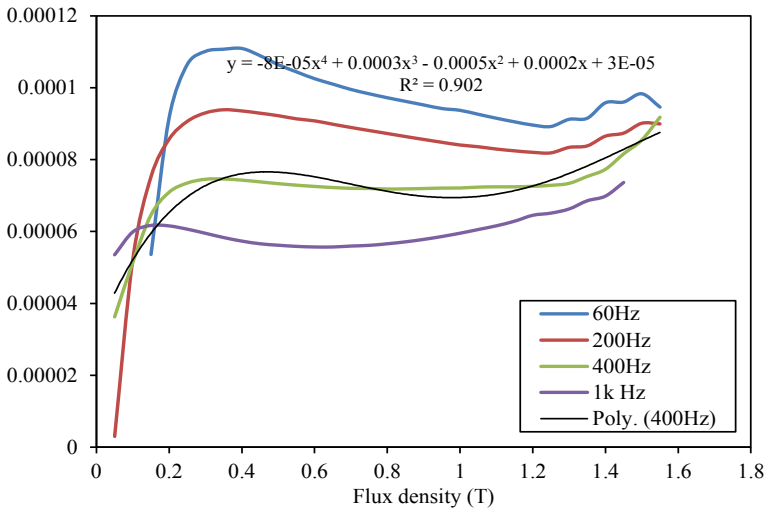

Fig 4.20 Eddy current coefficient vs flux density for M15G29.

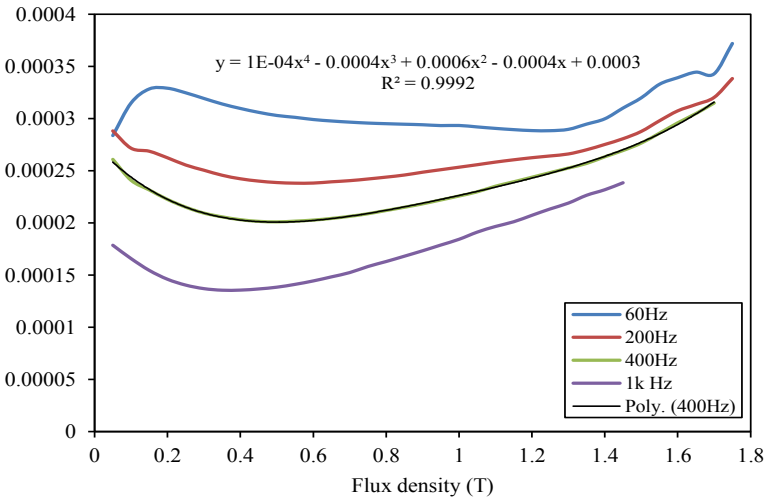

Fig 4.21 Eddy current coefficient vs flux density for M19G24.

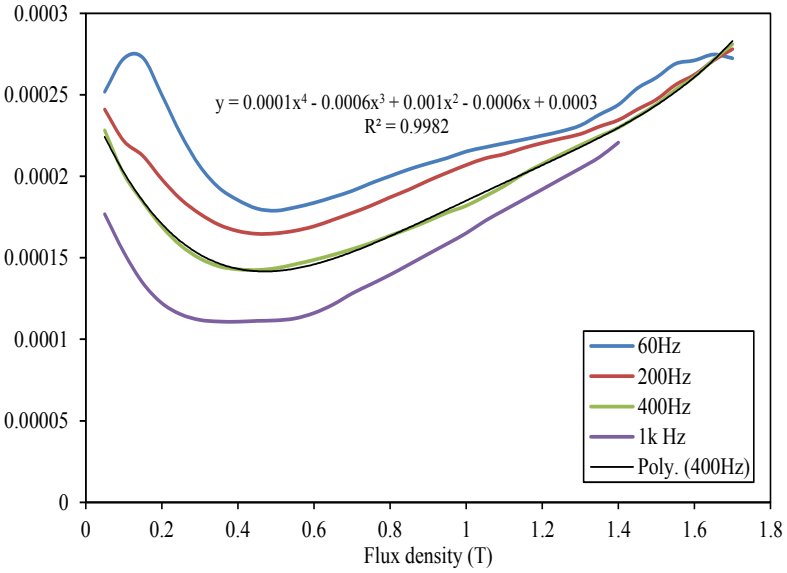

Fig 4.22 Eddy current coefficient vs flux density for M36G24.

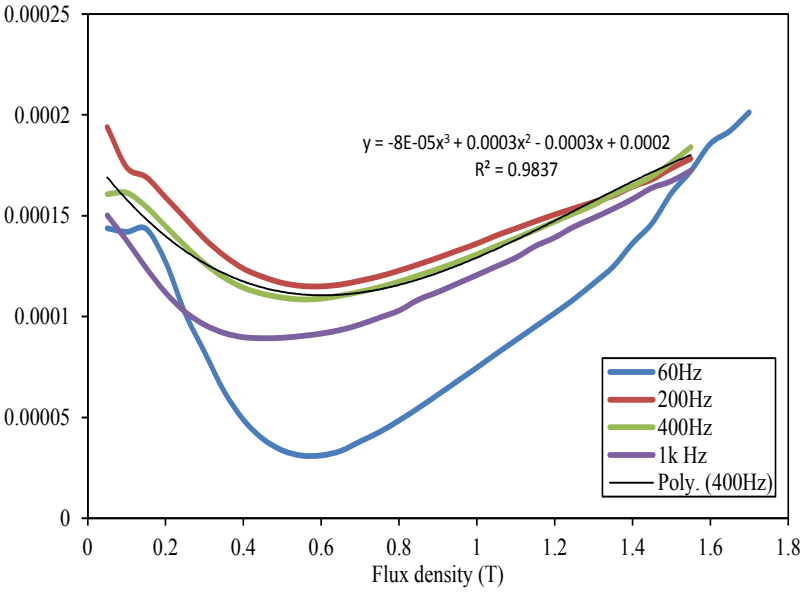

Fig 4.23 Eddy current coefficient vs flux density for M45G26.

4.3 Summary

In conclusion a new method of separation was used to gain more insight on the behavior of the core loss coefficients showing their dependence on frequency, flux density and material properties. The hysteresis coefficient was found to vary mostly in frequency and

almost constant with flux density. The eddy current and Steinmetz coefficients were found to vary with both frequency and flux density. These relationships proved true over different types of materials. In all the cases the outcomes obtained were in line with publications from other authors.

Chapter 5 Non-sinusoidal flux density core loss calculation.

Although all the measured core loss data used in machine design software is data obtained when laminations are excited with sinusoidal flux density waveforms, most machines because of their geometry and operation have non-sinusoidal flux. This means that the laminations in the machine core are exposed to non-sinusoidal flux density waveforms. Therefore using a core loss model for sinusoidal flux density waveform in many ways does not accurately predict the total losses in a real machine.

5.1 Flux density waveforms

The waveforms in different parts of a real machine are dependent on the geometry, type and operating conditions of the machine. Another source of non-sinusoidal flux density can be attributed to the drive. For example, the PWM inverter for induction machines. Because the inverter output is not purely sinusoidal it causes a distortion in the flux waveform. General core loss models [4] [33] [35] were proposed to enable core loss prediction with arbitrary and PWM voltage sources in the frequency and time domain. [27] summarizes the different methods and outlines how they can practically be used to calculate core losses. However most of these models have a dependency on the voltage source of the machine from which the flux density is dependent. Figs 5.1-5.4 show the flux waveforms at the stator yoke and stator tooth for permanent magnet synchronous machine with four poles, 24 slots at both no load and full load. Figs 5.5 and 5.6 show the flux density waveforms at the rotor pole and rotor core for a switched reluctance 6/4 machine operating at 900rpm. These figures therefore emphasize the need for a model that solves non sinusoidal flux density waveforms.

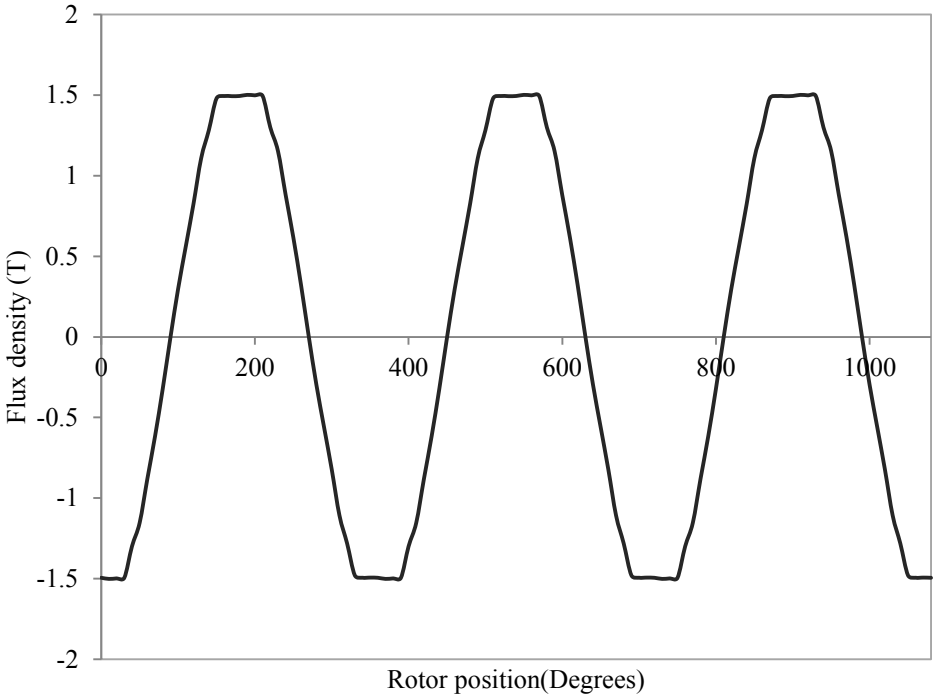

Fig 5.1 Flux density waveform at the stator yoke of a PM machine at no load.

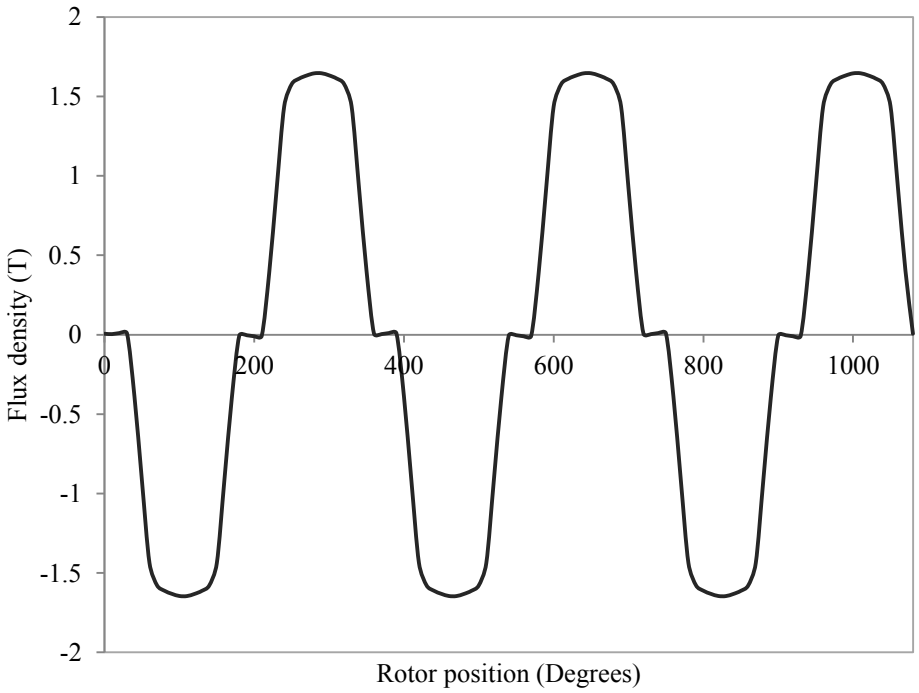

Fig 5.2 Flux density waveform at the stator tooth of a PM machine at no load.

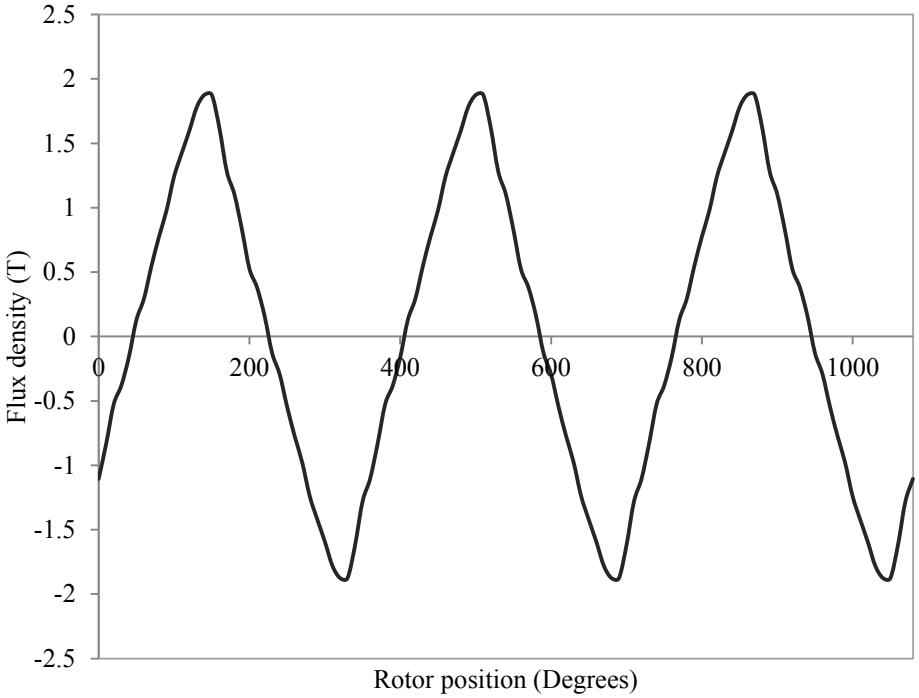

Fig 5.3 Flux density waveform at the stator yoke of a PM machine at full load.

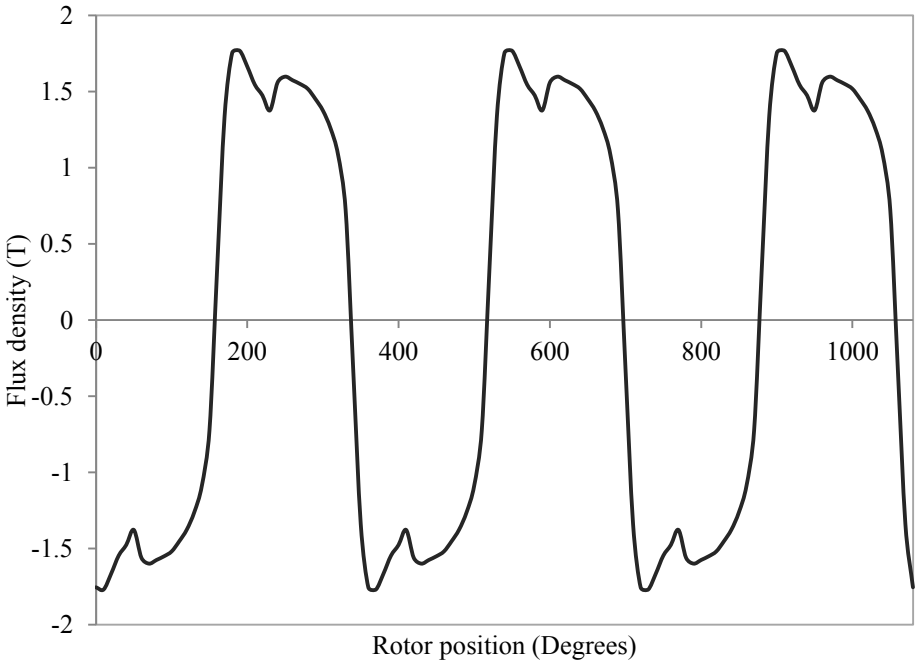

Fig 5.4 Flux density waveform at the stator tooth of a PM machine at full load.

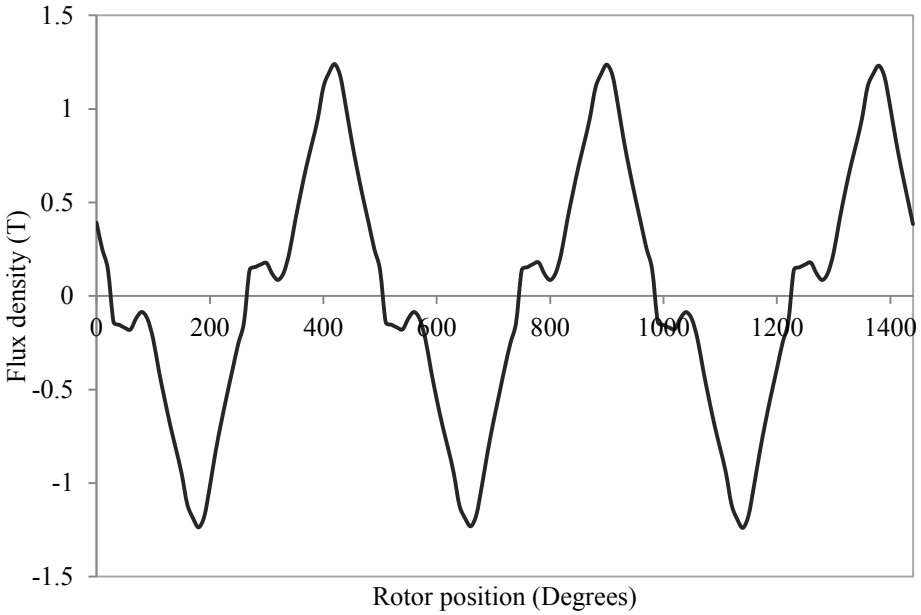

Fig 5.5 Flux density waveform at the rotor pole of a SRM.

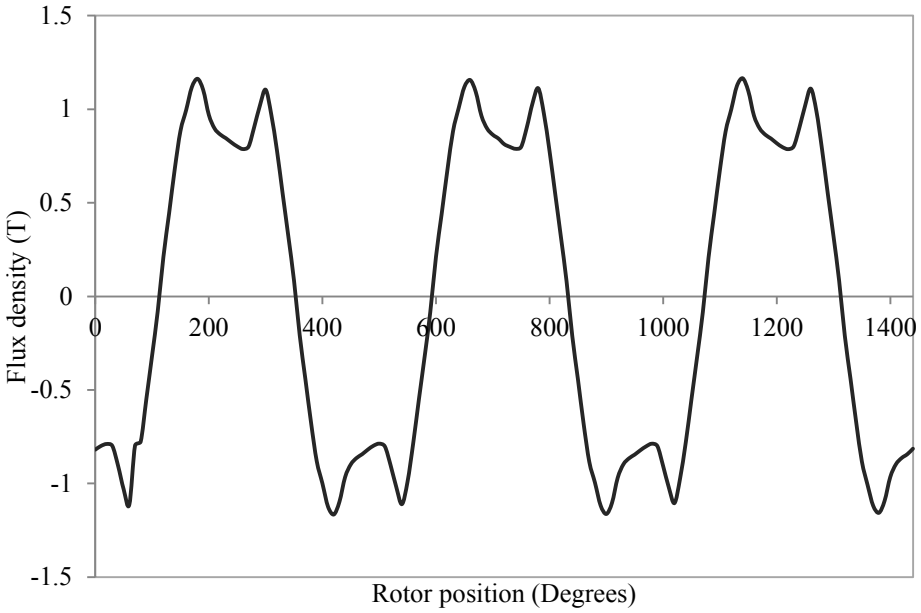

Fig 5.6 Flux density waveform at the rotor core of a SRM.

Core losses due to these waveforms are obtained by exciting the laminations with these exact waveforms and measuring the input current and output voltage on the secondary winding. This measured data is then used to validate the M formula when extended to non-sinusoidal flux density core loss prediction. Table 5.1 shows the comparison of the

measured losses using these non-sinusoidal waveforms to the purely sinusoidal waveforms having the same flux density peak and frequency for M19G24. The sinusoidal waveform loss underestimates the losses even though the flux density peak and frequency are the same with an error of up to 50%. This presented a need to extend the model to allow for accurate core loss prediction when exposed to non-sinusoidal flux density.

Table 5-1 Comparison of the non-sinusoidal waveform loss and its equivalent sinusoidal waveform loss

		B peak	Measured	Sine wave	Error (%)
PM-NL	Tooth	1.5	7.1	4.8	31.5
		1.2	4.1	2.8	31.5
		1	2.8	2.0	30.2
		0.8	1.8	1.3	28.8
	Yoke	1.5	5.4	4.8	10.8
		1.2	3.2	2.8	12.0
		1	2.2	2.0	11.5
		0.8	1.5	1.3	10.5
PM-FL	Tooth	1.5	10.2	4.8	52.6
		1.2	5.8	2.8	51.6
		1	3.9	2.0	49.4
		0.8	2.4	1.3	46.4
	Yoke	1.5	4.6	4.8	5.9
		1.2	2.6	2.8	5.9
		1	1.8	2.0	7.0
		0.8	1.2	1.3	7.4
SRM	RP	1.5	3.2	2.9	8.8
		1.24	2.0	1.8	7.8
		1	1.2	1.2	4.9
		0.8	0.9	0.8	7.5
	RC	1.5	4.6	2.9	36.2
		1.2	2.6	1.7	35.9
		1.16	2.4	1.5	36.2
		1	1.7	1.2	31.8
		0.8	1.2	0.8	33.9

5.2 Non-sinusoidal flux density implementation

Since the data available from manufactures is data obtained from exciting the lamination with a pure sinusoidal wave, using the M formula hysteresis loss, eddy current coefficient and excess loss coefficients under sinusoidal flux can be obtained. These values are later

used in the implementation for the non-sinusoidal flux density application. The M formula can be implemented in the frequency domain or the time domain to obtain the total core loss for non-sinusoidal flux density depending on the application and preference of the user.

5.2.1 Frequency domain

On the assumption that the fundamental component is most dominant, a non-sinusoidal waveform using Fourier analysis is a sum of sinusoidal waveforms. The fundamental and harmonic flux density magnitudes and frequencies are obtained from FFT analysis and used to calculate the eddy current loss and excess loss by adding the contribution of all the dominant harmonics as in (5.1) and (5.2). Fig 5.7 shows an FFT analysis for a stator tooth waveform from which the total core loss of the non-sinusoidal waveform is calculated. Only the most dominant components in the stem plot are used for the loss calculation using (5.3).

$$P_e = \sum_{n=1}^{d} K_{en}(nf)^2 {B_n}^2 \tag{5.1}$$

$$P_a = \sum_{n=1}^{d} K_{an}(nf)^{1.5} {B_n}^{1.5} \tag{5.2}$$

$$P_c = K_h f {B_p}^{(a+B_p b+c{B_p}^2)} + P_e + P_a \tag{5.3}$$

where d is the number of the highest order harmonic, n is the order of harmonic and B_p is the peak value of the waveform. The hysteresis loss component is only affected by the peak of the waveform and therefore the same as that of the sinusoidal waveform with the same peak.

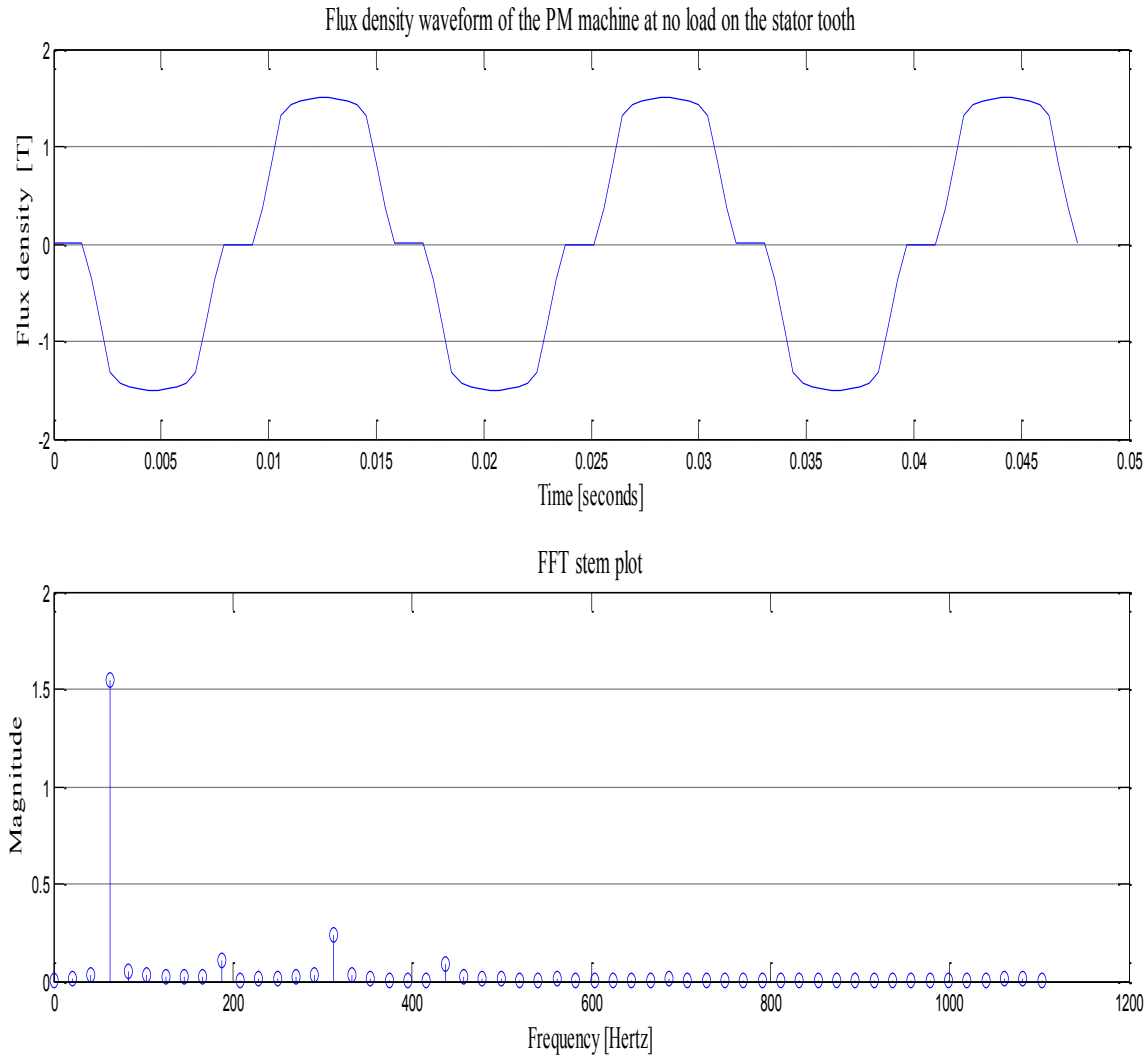

Fig 5.7 Flux density wave and its FFT showing the harmonics and their magnitudes

For each of the waveforms this procedure was followed to calculate the total core losses in the frequency domain.

5.2.2 Time domain

In [24] [25] [36] the time domain implementation is done for different models and results were presented showing good approximation of the losses.

Time domain implementation means converting the model such that it can calculate losses given a time dependent flux density waveform. The eddy current and excess loss

components are therefore converted into the time domain as shown in (5.4) from [37]. Since the hysteresis loss component is dependent on the peak flux density and not the flux waveform, the hysteresis loss can be calculated from the B peak.

$$P_c = P_h(B_p, f) + K_{et}\frac{1}{T}\int_0^T \left(\frac{dB}{dt}\right)^2 dt + K_{at}\frac{1}{T}\int_0^T \left|\frac{dB}{dt}\right|^{1.5} dt \quad (5.4)$$

Where $K_{et} = \frac{K_e}{(\sqrt{2}\pi)^2}$, $K_{at} = \frac{K_a}{(\sqrt{2}\pi)^{1.5}}$ and K_e is the eddy current coefficient at B peak during sinusoidal excitation and K_a is the excess loss coefficient at B peak during sinusoidal excitation. This time and frequency domain implementation was done for the SRM and PM machine waveforms for M19G24 and results presented in Table 5.2.

Table 5-2 Comparison of the time domain and frequency domain implementation of the M formula.

		B peak	Measured	Time domain	Error (%)	Frequency domain	Error (%)
PM-NL	**Tooth**	1.5	7.06	6.90	2.21	6.76	4.29
		1.2	4.09	4.03	1.28	4.13	1.04
		1	2.81	2.75	2.13	2.92	4.20
		0.8	1.82	1.76	3.46	1.94	6.63
	Yoke	1.5	5.42	5.38	0.75	5.17	4.70
		1.2	3.18	3.10	2.34	3.16	0.65
		1	2.21	2.14	3.12	2.25	1.83
		0.8	1.45	1.40	3.28	1.51	3.97
PM-FL	**Tooth**	1.5	10.03	9.26	7.64	9.22	8.08
		1.2	5.78	5.44	5.88	5.83	0.83
		1	3.87	3.65	5.75	4.15	7.31
		0.8	2.42	2.29	5.50	2.76	14.06
	Yoke	1.5	4.56	4.59	0.54	4.74	3.76
		1.2	2.64	2.61	1.30	2.61	1.40
		1	1.83	1.81	1.18	1.79	2.33
		0.8	1.21	1.20	1.07	1.17	3.03
SRM	**RP**	1.5	3.22	3.19	1.12	3.41	5.82
		1.2	1.99	1.97	0.81	2.01	1.25
		1	1.24	1.27	2.29	1.25	0.89
		0.8	0.85	0.84	1.61	0.81	4.41
	RC	1.5	4.61	4.25	7.73	4.37	5.20
		1.2	2.62	2.54	3.02	2.60	0.85
		1	1.73	1.78	2.56	1.83	5.53
		0.8	1.19	1.16	2.32	1.21	5.53

Generally both implementations give good loss prediction with acceptable errors. Fig 5.8 - Fig 5.10 show the comparison of the measured and calculated loss for the waveforms tested.

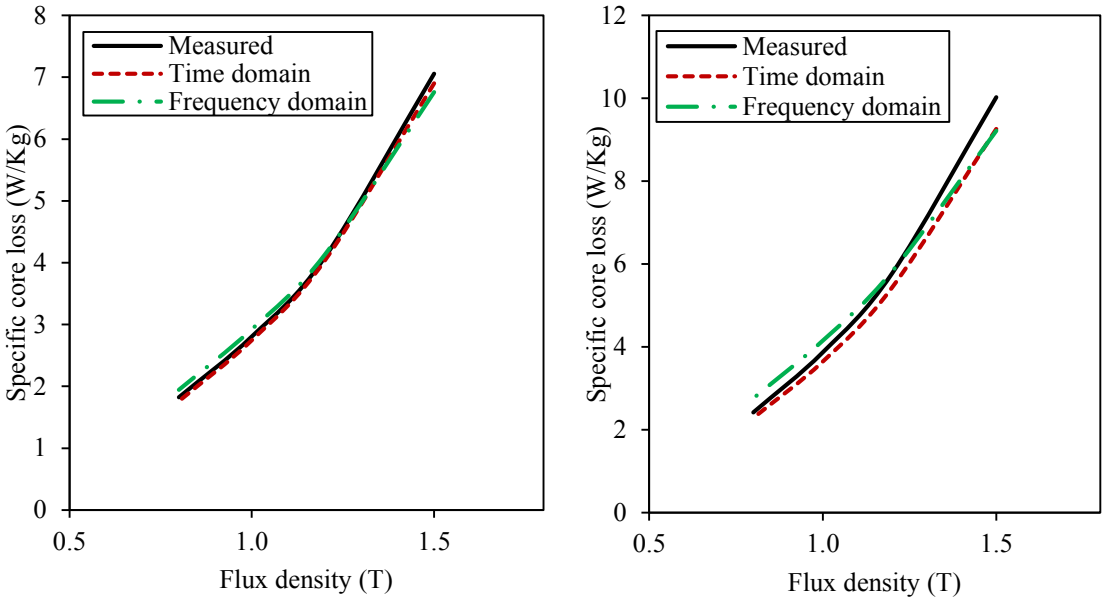

Fig 5.8 Calculated and the measured loss for the PMSM stator tooth waveform at no load and full load

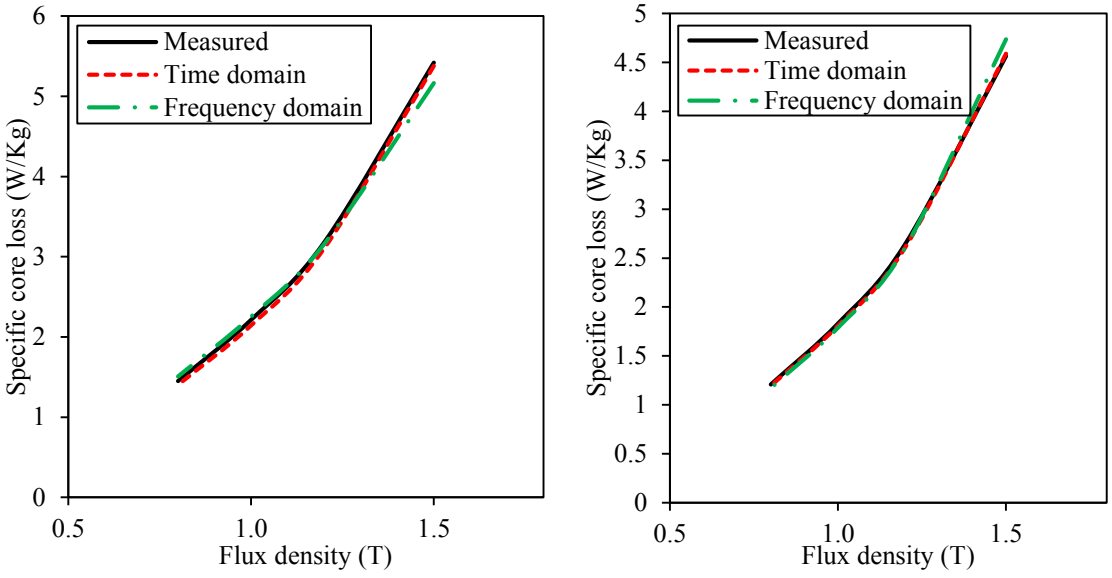

Fig 5.9 Calculated and measured loss for the PMSM stator yoke waveform at no load and full load

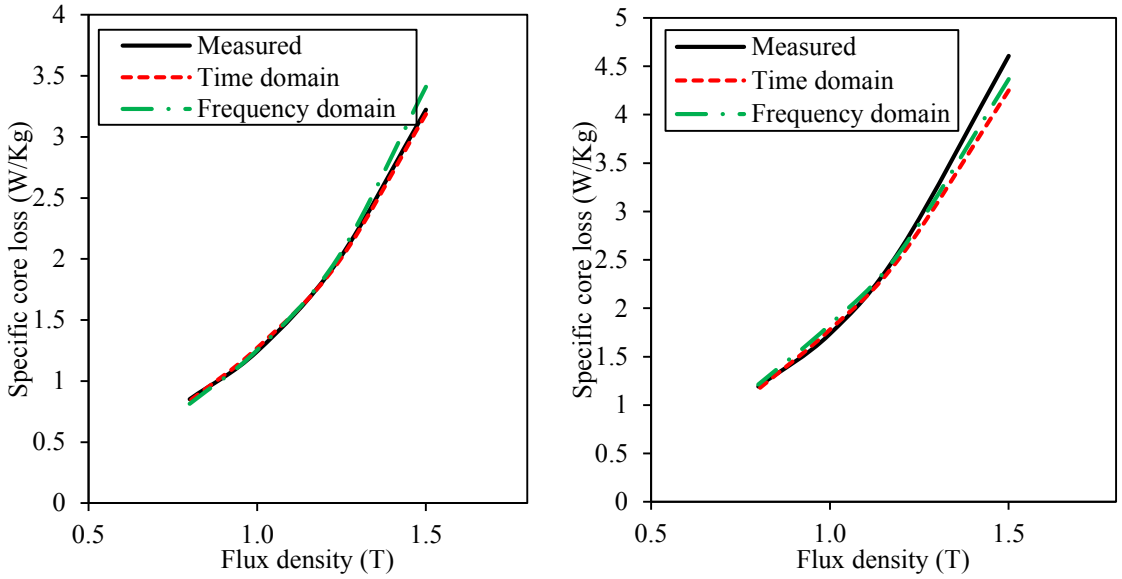

Fig 5.10 Calculate and measured loss for SRM at the rotor pole and rotor core waveforms

It was noted for both implementations that waveforms with flux reversals generally gave a higher percentage error greater than 5% with the error even higher at higher peak flux densities. The time domain implementation showed better prediction of the non-sinusoidal flux density waveform with maximum error less than 10%. Both methods can be improved to better predict the losses.

Frequency domain implementation – increasing the harmonic spectrum considered in the calculation gives a better representation of the non-sinusoidal waveform therefore predicting the losses better.

Time domain implementation – for better numerical evaluation of the eddy current and excess loss components, smaller time steps can be used. A more accurate minor loop correction factor for the hysteresis loss can improve on the calculated error.

The time domain implementation finds application in machine design software or calculation of the total core loss in a machine using finite element method.

5.3 Minor loop correction

Flux reversals occurring in the waveforms indicate the presence of minor loops, the larger the flux reversal, the bigger the minor loop. These minor loops also contribute to the total hysteresis loss in the material depending on their magnitude hence the need to correct for them in core loss formulas. In the time domain, a correction factor needs to be added for minor loops especially if the loops are large and can affect the total loss. In frequency domain however these reversals from the FFT are interpreted as harmonics and therefore factored in the loss calculation.

In [38] a correction factor for minor loops was proposed, this correction factor was reported to ideally be a function of the magnitude of the flux reversal, position of the minor loop and the peak of the waveform. However since they could not find an equation combining all the above factors, the authors derived this correction factor (5.5) after analysis of some experimental minor loop measurements [39].

$$P_h = P_{hsine}(1 + k * \Delta B_T) \tag{5.5}$$

$$\Delta B_T = \frac{1}{B_p} \sum_{i=1}^{N} \Delta B \tag{5.6}$$

Where only flux reversals in the positive half cycle are considered and ΔB is the magnitude of the flux reversal, k was found to be 0.6-0.7 depending on the material used. [40] found k = 0.8 for SRM from experimental measurements.

More recently [41] [42] [43] suggested a scaling power law (5.7) for both asymmetrical and symmetrical minor loops therefore disregarding the importance of minor loop position.

$$W_F^* = W_F^0 \left(\frac{M_a^*}{M_s}\right)^{nF} \tag{5.7}$$

Where W_F is the minor loop hysteresis loss, W_F^0 reflects the material's properties including defect density, magnetocrystalline anisotropy and intern stress, M_a^* is the minor loop flux density, M_s is the saturation magnetization of this steel, nF is a constant and almost independent of temperature, stress and types of ferromagnets. The authors in their subsequent papers reported $nF = 1.44 \pm 0.06$. W_F^0 was determined from fitting minor loop data to (5.7) therefore obtaining $W_F^0 = 0.02073$.

Both correction factors were applied on the stator tooth waveform at full load and the SRM waveforms exhibiting flux reversals. Table 5-3 shows a comparison of the two correction methods with the measured loss and the calculated uncorrected loss.

Table 5-3 Effect of the correction factor

	Uncorrected Error(%)	Eqn (5.4) Error(%)	Eqn(5.6) Error(%)
PM-FL Stator tooth	7.64	6.88	7.63
	5.88	5.44	5.88
	5.75	5.40	5.75
	5.50	5.15	5.49
SRM Rotor pole	1.12	1.21	1.11
	0.81	0.73	0.79
	2.29	3.46	2.30
	1.61	0.60	1.59
SRM Rotor Core	7.73	1.06	7.67
	3.02	1.03	2.95
	2.56	5.99	2.64
	2.32	0.62	2.24

It was observed that these correction factors had very little effect on the minor loop correction this was mainly because the size of the minor loops were very small therefore had minimum effect on the total hysteresis loss and hence the total core loss.

Improvement of this loss therefore goes back to the accuracy of the integration and differentiation.

5.4 Machine stator core

The model is applied to a real machine stator core. This is done by modeling the machine stator in finite element software, obtaining the flux density in the core and calculating the losses using the suggested model. Fig 5.11 shows the wound machine core ready for core loss measurement and a model of the core in Finite Element Method Magnetics FEMM [44].

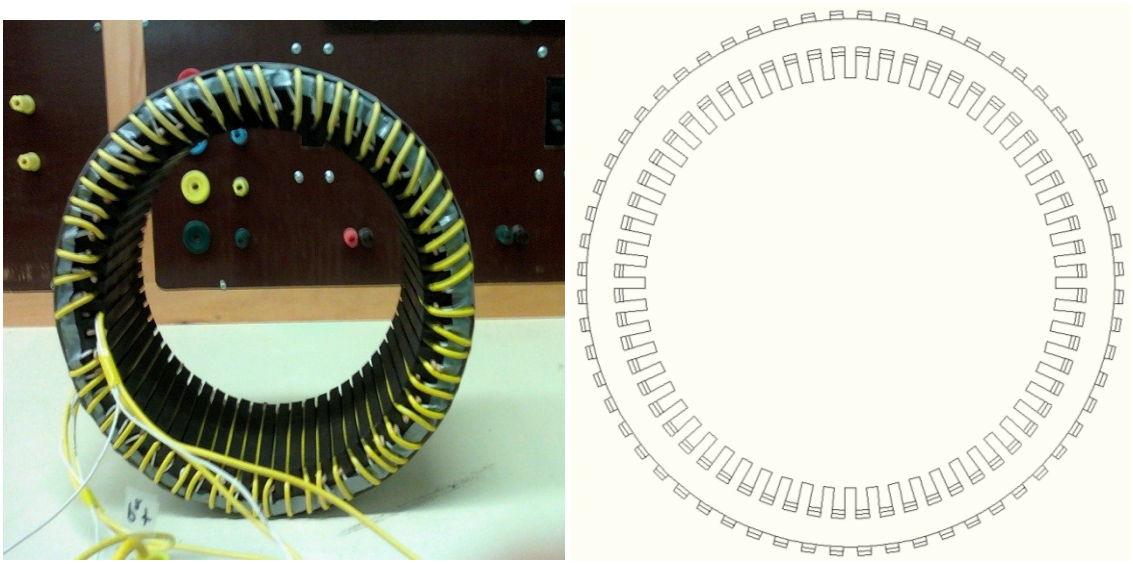

Fig 5.11 Typical stator core and its model in FEMM

Core losses in the stator core above are measured at different operating points and this data was used to validate the FEMM model. A given current in the primary windings produces a certain flux in the machine core therefore if this same current is set in the machine model, the flux density obtained should also be the same. This was obtained by changing the B-H curve in the software to the B-H of the frequency being tested. From the simulation, the flux density distribution was limited to the core of the stator as

observed in Fig 5.12. It is worth mentioning that the losses in the stator of the core represent only a section of the total core losses in the real machine since the losses in the stator teeth are not included.

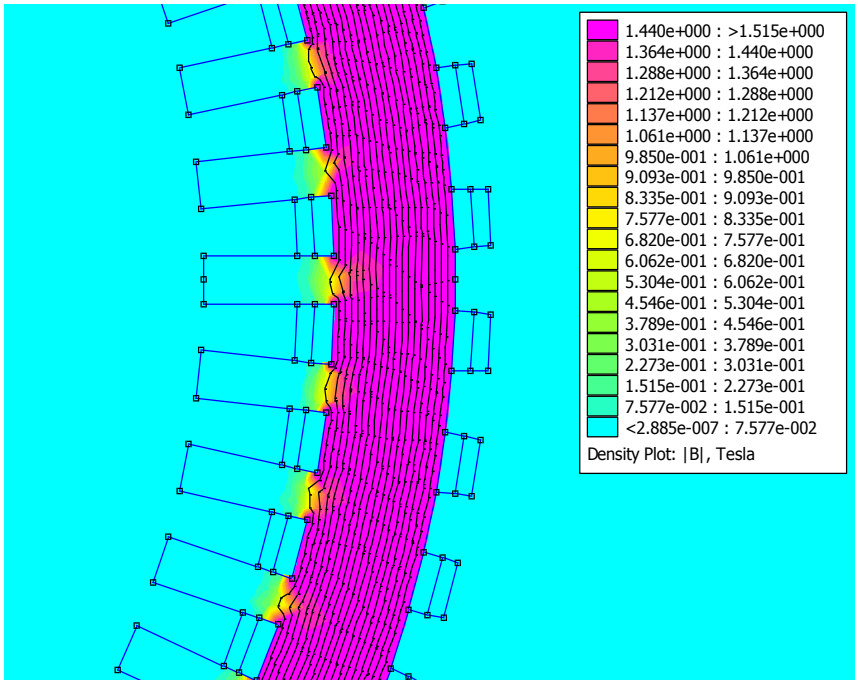

Fig 5.12 Flux density distribution in the stator.

With the flux density known total losses in the core can be calculated using either the frequency or time domain implementation. Fig 5.13 shows the results obtained when the measured loss, the loss obtained from the model and the loss from Epstein measurements are compared. Results obtained were consistent with the Epstein results mainly because the coefficients used were obtained from the Epstein measurements. When the coefficients are calculated from core loss data of the machine core, the results show good prediction with percentage error less than 5%. This implies that a model is only as good as the data from which its coefficients are derived. In this case a stress correction factor of 1.23 was obtained between the Epstein results and the measured results. When this

factor is added to the model results or the Epstein results, the losses are sufficiently predicted. To effectively determine this stress factor for different machines, one has to model the stress factor in relation to different manufacturing processes of the machine. This factor can then be added to the core loss formula obtained from Epstein results. This is important because the data in machine design software (Epstein data) does not effectively represent the losses in the real core.

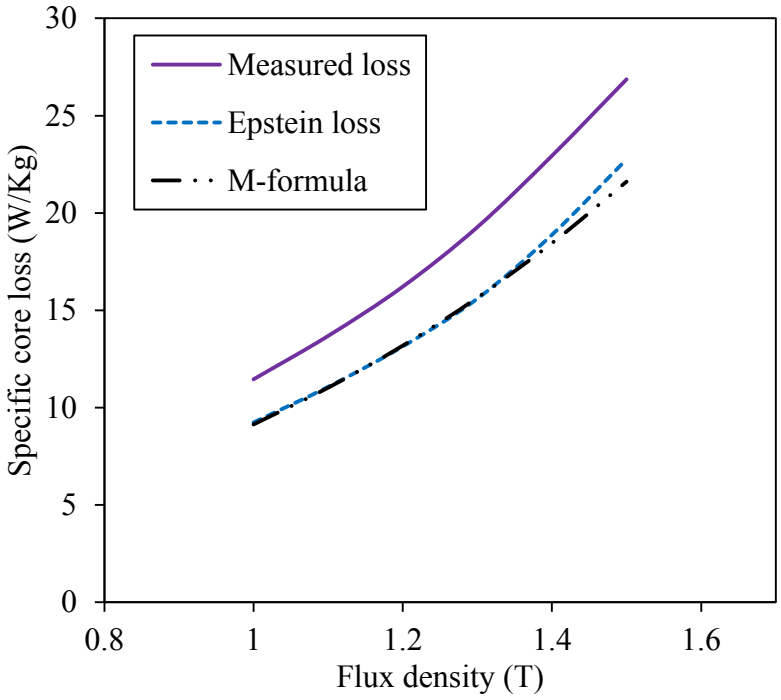

Fig 5.13 Machine stator core losses

Although this model can be used to effectively predict core losses, it does have some limitations;

- Being a best fit model, it is limited to data used in the fitting. Data out of the range cannot be sufficiently predicted.

- Material behavior and properties are lost in this loss calculation approach since all these physical characteristics (stress, domain behavior) cannot be modeled by linear and curve fitting algorithms.

5.5 Summary

The M formula has been extended to allow core loss calculations under non-sinusoidal flux density excitation. This has been implemented in both the time domain and the frequency domain and their results were presented.

Chapter 6 Conclusion

Energy efficiency is a priority hence an interest in core losses in machines. Various core loss formulas have been developed from modifications of the Steinmetz equation with dependence on experimental data to model and predict core losses. Since core losses are material specific, measurements are made on four types of materials with different magnetic properties.

A commercial test bench is used to collect core loss data at various frequencies and flux densities of the different materials. This data is obtained using different core loss testers. It was found that the total core loss obtained from the toroid tester was higher than the loss obtained for the same material using the single sheet tester and the Epstein tester. This was mainly attributed to the stress experienced by the toroid sample which was validated by their permeability curves.

An in depth review of some of the formulas used to predict core losses including their algorithms is done in chapter 3 and a new model proposed. All the models presented were tested for accuracy by comparing the calculated loss with the measured loss. The proposed model apart from being comparable with other models in terms of the accuracy also enables core loss prediction at higher frequencies and flux densities. Its performance at frequencies of 2 kHz and 4 kHz showed its suitability for extension to high frequencies. All this is achieved with a somewhat simple algorithm that can be implemented in a spread sheet.

Although the methods reviewed presented a good correlation between the measured and calculated loss, the method of loss separation used was based on the loss extrapolation to

zero frequency which is usually true at low frequencies when there is no skin effect. At higher frequencies when skin effect is present, extrapolation underestimates the hysteresis loss therefore affecting the values of the loss coefficients. Using a new method of loss separation that takes into account skin effect, the behavior of the hysteresis loss, eddy current loss and the Steinmetz coefficients are studied and relationships obtained showing that these coefficients rather than being constant are functions of frequency and flux density. This analysis was done on data obtained from the experimental measurements using all the three testers. Results also showed that this method of separation was more evident in the single sheet and Epstein testers while the toroid tester showed that even at higher frequencies the hysteresis loss was the same as that obtained at lower frequencies.

This model was extended to evaluate the core losses due to non-sinusoidal flux density waveforms that occur in real machines. The flux density distribution waveforms tested were those obtained from different parts of the permanent magnet machine and switched reluctance machine simulation in different operating conditions. Non-sinusoidal flux density core loss calculation was implemented in both the frequency and time domains. Losses due to these non-sinusoidal waveforms were obtained by exciting the primary coil with these waveforms and measuring the losses. In the comparison of the calculated losses and the measured losses, results obtained showed acceptable errors when the model was implemented in both domains.

6.1 Future work

- Implementation of this model in a machine design software to calculate the total core losses.
- Using more physical based methods for loss calculations to obtain a more general model.

References

[1] T Litman, *Efficient Electric Motor Systems Handbook*.: The Fairmont Press, INC,Oklahoma, 1995, pp. 21-37.

[2] Todd Litman, John G.Douglas and G.A McCo, *Energy-Efficient Electric Motor Selection Handbook*., January 1993, p. 11.

[3] C.P Steinmetz, "On the law of hysteresis (originally published in 1892)," *Proc. IEEE*, vol. 72, no. 2, pp. 196-221, 1984.

[4] A. Boglietti, A. Cavagnino, M. Lazzari and M. Pastorelli, "Predicting Iron losses in soft magnetic materials with arbituary voltage supply: An engineering approach," *IEEE Transactions on magnetics*, vol. 39, no. 2, 2003.

[5] Pragasen Pillay, "Improved Design of Motors for increased Efficiency in Residential and Commercial Buildings," Clarkson University, Potsdam, Department of Energy Report 2008.

[6] P.H Pry and C.P Bean, "Calculation of the energy loss in magnetic sheet materials using a domain model," *Journal of applied physics*, pp. 532-533, 1958.

[7] H. Hauser, "Energetic model of ferromagnetic hysteresis: Isotropic magnetization," *Journal of Applied Physics*, vol. 96, no. 5, p. 2753, 2004.

[8] D.C Jiles and D.L Atherton, "Theory of ferromagnetic hystersis," *J. Magnet. Magn. Mater.*, vol. 61, pp. 48-60, 1986.

[9] E.D Torre, *Magnetic Hystersis*. New york: IEEE Press, 1999.

[10] AK Steel, "Selection of electrical steels for magnetic cores," AK Steel Corporation, Product Data Bulletin 2007.

[11] ASTM Standard A348/A348M-00, "Standard Test method for Alternating Current magnetic properties of materials Using the Wattmeter-Ammeter-Voltmeter Method, 100 to 10 000Hz and 25-cm Epstein Frame," West Conshohocken,PA, DOI: 10.1520/A0348_A0348M-00, 2000.

[12] IEC 60404-2, "Magnetic materials. Part 2: Methods of measurement of the magnetic properties of electrical steel sheet and strip by means of an Epstein frame," Edition 03, ICS 20.030, 2008.

[13] IEC 60404-3, "Magnetic materials - Part 3: Methods of measurement of the magnetic properties of magnetic sheet and strip by means of a single sheet tester.," Edition 02, ICS

29.030, 2002.

[14] "Lamination steels types,properties and specifications. A compendium of lamination steel alloys commonly used in electrical motors," 2000.

[15] (1999-2010) Model 3110-MS2 Computer Controlled Magnetic Test Console. [Online]. http://www.donartelectronics.com/ms2.html

[16] ASTM Standard A348/A348M-05, "Standard test method for alternating current magnetic properties of materials using the wattmeter-ammeter-voltmeter method, 100 to 10000Hz and 25cm Epstein frame," West Conshohocken,PA, DOI: 10.1520/A0348_A0348M-05 , 2000.

[17] ASTM Standard A927/A927M-99, "Standard test method for alternating current magnetic properties of Toroidal core specimens using the voltmeter-ammeter-wattmeter method," West Conshohocken, PA, DOI: 10.1520/A0927_A0927M-99, 1999.

[18] ASTM A804 / A804M - 04(2009)e1, "Standard test methods for alternating-current magnetic properties of materials at power frequencies using sheet type test specimens," West Conshohocken, DOI: 10.1520/A0804_A0804M-04R09E01, 2009.

[19] P. Pillay and L.T Mthombeni, "Core losses in motor laminations exposed to high frequency or non-sinusoidal excitation.," *IEEE Trans. Ind.App*, vol. 40, no. 5, pp. 1325-1332, 2004.

[20] Maged Ibrahim and Pragasen Pillay, "Novel equipment for the measuremetn of core losses in laminations for advanced machines.," in *IEEE IEMDC*, 2011.

[21] "Switched reluctance motor simulation software," Motorsoft INC, User Manual PC-SRD 4.7 Motorsoft INC.

[22] Yicheng Chen and Pragasen Pillay, "Am Improved Formula for Lamination Core loss Caculations in Machines Operating with High Frequency and High Flux Density Excitation," in *IEEE 37th IAS Annunal Meeting Conference*, Pittsburgh, 2002.

[23] M. Popescu, S.J Dellinger, T.J.E. Miller, R.J. Heideman and McGilp D.M Ionel, "On the variation with flux and frequency of the core loss coefficients in electrical machines.," *IEEE Trans. Ind.Appl*, pp. 658-667, 2006.

[24] D.M Lonel et al., "Computation of Core losses in electrical machines using improved models for laminated steel.," *IEEE Trans.Ind.Appl.*, vol. 43, no. 6, Nov/Dec 2007.

[25] M. Popescu, S.J. Dellinger, T.J.E. Miller, R.J. Heideman and M.I. McGilp D.M. Ionel, "Factors affecting the acuurate prediction of core losses in electrical machines," Glasgow,UK, 2005.

[26] T.L Mthombeni and P. Pillay, "Physical basis for the variation of lamination core loss coefficients as a function of frequency and flux density," in *IECON*, 2006.

[27] A. Boglietti and A. Cavagnino, "Iron loss prediction with PWM supply: An overview of proposed methods from an engineering application point of view," in *IEEE IAS*, 2007.

[28] H. Pfutzner, P. Schonhuber, B. Erbil, G. Harasko and T. Klinger, "Problems of loss seperation for crystalline and consolidated amorphous soft magnetic materials.," *IEEE Transactions on Magnetics*, vol. 27, no. 3, pp. 3426-3432, 1991.

[29] Mircea Popescu and Dan Ionel, "A best fit model of power losses in cold rooled-motor lamination steel operating in a wide range of frequency and magnetization.," *IEEE Trans.Mag*, vol. 43, no. 4, 2007.

[30] M. Ibrahim and P.Pillay, "Advanced testing and modeling of magnetic materials including a new method of core loss separation for electrical machines.," in *IEEE Energy Conversion Congress and Exposition*, Sept 2011.

[31] T.L Mthombeni, P.Pillay, A. Boglietti and M.J Manyage, "Improved prediction of core losses in induction motors.," in *IEEE EMDC*, 2007.

[32] G. Bertotti, "General properties of power losses in soft ferromagnetic materials," *IEEE Trans. Magnetics*, vol. 24, no. 1, pp. 621-630, 1988.

[33] M. Amar and R. Kaczmarek, "A general formula for prediction of Iron losses under nonsinusoidal voltage waveform.," *IEEE Trans.Mag*, vol. 31, no. 5, pp. 2504-2509, 1995.

[34] D.M Ionel, A. Boglietti, A Cavagnino, C. Cossar and McGilp M. Popescu, "A general model for estimating the laminated steel losses under PWM voltage supply," *IEEE Trans.Ind.App*, vol. 46, no. 4, pp. 1389-1396, 2010.

[35] D.M. Ionel et al., "A general model for estimating the laminated steel losses under PWM voltage supply.," *IEEE Trans.Ind Apps*, vol. 46, no. 4, pp. 1389-1396, 2010.

[36] P. Pillay and Marubini J Mannyage, "Low voltage high current PM traction motor design using recent core loss results," in *IEEE Industry Applications conference*, 2007.

[37] Manyage M.J, T.L Mthombeni, and P.Pillay, "Improved prediction of core losses in induction motors," in *IEEE, IEMDC*, 2007.

[38] J.D Lavers, P.P Biringer, and H. Hollitscher, "A simple method of estimating the minor loop hysteresis loss in thin laminations.," *IEEE Trans. on magnetics*, vol. 14, no. 5, 1978.

[39] T. Nakata and Y. Ishihara, "Experimental studies of various factors affecting minor loop hysteresis loss," *Memoirs of the school of engineeing,okayama university*, June 1973.

[40] Y.Hayashi and T.J.E Miller, "A new approach to calculating core losses in the SRM," *IEEE. Trans.Ind Appl*, vol. 31, no. 5, pp. 1039-1046, 1995.

[41] Satoru Kobayashi and Seiki Takahashi, "Scaling power-law relations in asymetrical minor hysteresis loops.," *Journal of applied physics*, vol. 107, no. 6, March 2010.

[42] Satoru Kobayashi, Seiki Takahashi, Yasuhiro Kikuchi and Kamada Hiroaki, "A Low-Field Scaling Rule of Minor Hystersis Loops in Plastically Deformed Steels," *IEEE Transactions on magnetics*, vol. 46, no. 2, pp. 191-194, February 2010.

[43] Satoru Kobayashi, Atsushi Saito, Seiki Takahashi, Yasuhiro Kamada and Hiroaki Kikuchi, "Characterization of Strain-induced Martensite Phase in Austenitic Stainless Steel using a Magnetic Minor-loop Scaling Relation," *Journal of Applied physics Letters*, vol. 92, no. 18, May 2008.

[44] David Meeker, Finite Element Method Magnetics Software, 2010, FEMM Version 4.2.

[45] J. Sievert, "The measurement of magnetic properties of electrical sheet steel-survey on methods and situation of standards," *Elsevier-Journal of Magnetism and Magnetic Materials*, vol. 215-216, pp. 647-651, 2000.

[46] J. Sievert, H.Ahlers, P.Brosien, M.Cundeva and J.LuedKe, "Relationship of Epstein to SST results for Grain Oriented Steel.," in *Non-Linear Electromagnetic systems: ISEM'99*.: IOS Press, 2000, pp. 3-6.